Department of Precision and Microsystems Engineering

Non-enzymatic electrochemical sensing of glucose with nano-structured and functionalised diamond electrodes

Heleen Payens

Report no	: 2017.042
Coach	: Dr. J.G. Buijnsters & Dr. A.F. Sartori
Professor	: Prof.dr.ir. G.C.A.M. Janssen
Specialisation	: Micro and Nano Engineering
Type of report	: Master Thesis
Date	: 28-09-2017

Non-enzymatic electrochemical sensing of glucose with nano-structured and functionalised diamond electrodes

by

Heleen Payens

to obtain the degree of Master of Science
at the Delft University of Technology,
to be defended publicly on Wednesday October 11, 2017 at 09:30 AM.

Student number:	1512382	
Project duration:	September 1, 2016 – October 11, 2017	
Thesis committee:	Prof. dr. ir. G. C. A. M. Janssen	TU Delft, PME
	Dr. J. G. Buijnsters	TU Delft, PME
	Dr. Y. Gonzalez-Garcia	TU Delft, MSE
	Dr. A. F. Sartori	TU Delft, PME

An electronic version of this thesis is available at `http://repository.tudelft.nl/`.

Preface

After one year of doing my thesis project, it is time to graduate. Several times people were surprised about my research subject in combination with my mechanical engineering studies. I have always loved the broad and extensive subjects that fit into mechanical engineering. I look back on this year with satisfaction and pride. I dived into a total new area for me, which was really challenging. This made the work very interesting and helped me keeping my head straight. Ivan and André helped me a lot during my project, which I am very grateful for. I also want to thank my friends, family, fellow students in the office and other fellow students for all support during my whole studies. All this work could not have been done without the help of all of you. Not everything always worked out the way you wish, but in life you have to deal with these things. Attached poem from Toon Hermans always helped me through busy periods during my study. Therefore, I would like to share this with you. At the end, everything's gonna be all right.

Figure 1: Poem written by Toon Hermans

Heleen Payens
Delft, September 2017

Abstract

Electrochemical sensing is a powerful tool for the rapid detection of (bio)molecules in fluids, and is frequently used in clinical analysis and diagnostics. Diamond is arguably the best electrode material for its robustness, wide potential window, very low background current, biocompatibility and self-cleaning features. Nowadays, there is a new trend leading to electrodes getting smaller. One of the current challenges in the development of diamond micro-electrodes is to increase the sensitivity of the diamond electrode, while the electrode's dimensions decrease. An interesting biomolecule to detect is glucose. 2.8% of the world population suffers from diabetes, these people need to measure their blood sugar level and manage this level by dispensing insulin in their body when needed. A glucose sensor is used to determine the amount of glucose in the blood. Boron-doped diamond (BDD) is an interesting material for the non-enzymatic detection of glucose. In this thesis project, study has been done to the nanostructuring and functionalisation effects on the performance of sensing glucose by using diamond electrodes. Measurements have been done with different types of electrodes: bare BDD, acid cleaned BDD, BDD functionalised with gold nanoparticles, BDD with a nanowire surface structure, and BDD with a nanowire surface structure and gold nanoparticles on top. It was found possible to detect glucose with three of these samples: bare BDD, BDD with gold nanoparticles, and the nanostructured BDD functionalised with the gold nanoparticles. The other two electrode types did not give any reduction/oxidation peaks, which is attributed to the oxygenated surface resulting from their fabrication processes. The three glucose-detecting electrodes showed linear behaviour in a range of 1-10 mM, which is in line with the detection range of glucose in human blood. The sensitivities achieved with bare BDD, BDD with gold nanoparticles, and the nanostructured BDD functionalised with the gold nanoparticles are 0.022, 0.429, and 0.136 $mA/mMcm^2$, respectively. The addition of gold particles improves the sensitivity for glucose substantially and works like an electrocatalyst. Making use of electrocatalysts is an interesting and useful functionalisation for direct non-enzymatic glucose sensing, because sensing glucose with bare BDD is a kinetically very slow process. Results of such high sensitivities for BDD with gold nanoparticles were not published in literature yet, so this is a promising achievement that asks for continuation of research in this field.

Contents

1 Introduction

Electrochemical sensing is a simple and fast way to detect and measure (bio)molecules accurately in fluids and is of importance in clinical analysis and diagnostics, food safety control, water pollution, and many more applications.

Diamond is an excellent electrode material because of its great electrochemical properties. It has a wide potential window, high resistance to fouling and corrosion, high electric conductivity when doped with boron, it is biocompatible and it has a very low background current.

Diamond electrodes are already being used. A lot of research has been done on different dopant types, different dopant concentrations and the influence of crystallographic orientation on its' sensing properties.

Nowadays, there is a new trend leading to electrodes getting smaller. One of the current challenges in the development of diamond micro-electrodes and micro-electrode arrays is to increase the sensitivity of the diamond electrodes, while the electrode's dimensions decrease.

It is possible to improve the sensitivity of electrodes by nanostructuring the surface and/ or adding surface modifications. With nanostructuring, structures are created on the diamond's surface. For instance, nanowires or nanocylinders are produced on the initially flat electrode surface. This increases the surface area of the electrode and possibly also its sensitivity. With surface modifications, functional chemical groups containing hydrogen or oxygen can be added to change the surface properties thereby increasing the sensitivity for specific target molecules.

2.8% of the world population suffers from diabetes, a disease where the own body is not able to manage the blood sugar levels itself. Diabetics need to measure their blood sugar level and manage this level by dispensing insulin in their body when needed. A glucose sensor is used to determine the amount of glucose in the blood. There are two types of glucose sensors: non-enzymatic and enzymatic sensors. Enzymatic glucose sensing with the enzyme glucose 1-oxidase (GOx) is used mostly these days. Advantages of GOx are the high selectivity, high sensitivity and good stability compared to other enzymes. A big disadvantage is the instability of enzymes, the enzymes are effected a lot by ambient conditions. With non-enzymatic glucose sensing, the glucose is detected directly. Advantages of the non-enzymatic glucose sensors are that it is stable, simple and has low production costs. Boron-doped diamond can also be used in harsh environments. This makes the non-enzymatic detection of glucose very attractive.

The goal of this thesis is to electrochemically characterise nanostructured and surface-modified boron-doped diamond (BDD) electrodes and see which sensitivities for non-enzymatic glucose sensing can be achieved with these electrodes. Comparison will be made with as-grown BDD electrodes. The characterisation of the BDD electrodes will be done by scanning electron microscopy, raman spectroscopy, cyclic voltammetry, and electric impedance spectroscopy.

First, the literature study will be discussed in Chapter 2, then, the research area of focus is described in Chapter 3. In Chapters 4 and 5, the experimental work and the accompanying results are handled. The conclusions can be found in Chapter 6. Finally, some recommendations for future research will be given in Chapter 7.

2

Literature review

All relevant literature for this thesis will be discussed in this chapter. First, diamond's material properties and synthesis methods will be explained in Section 2.1. Second, diamond electrodes and the structuring and modification of these are discussed in Section 2.2. The characterisation techniques are explained in Section 2.3. The electrolytes used are described in Section 2.4 and, finally, diamond electrode use as glucose sensors is discussed in Section 2.5.

2.1. Diamond

2.1.1. Material properties

Diamond is an allotrope of carbon and it is the hardest bulk material in the world. This great hardness is due to its lattice structure. The unit cell of diamond contains 8 carbon atoms, arranged in a cube, as shown in Figure 2.1a. Each carbon atom is joined to 4 other carbon atoms by covalent bonds which have a tetrahedral orientation, as shown in Figure 2.1b. The carbon atoms are equidistant from each other and the atomic configuration is stable and very rigid[1]. Diamond has also other favourable properties: it has a high thermal conductivity and extremely low thermal expansion coefficient. It has a high abrasive wear resistance, it is chemically inert to most acids and alkalis, it is transparent in a wide wavelength range, it has a low work function, it is minimally compressible and has a very high stiffness[2, 3]. A short-list of the material properties of diamond with reference to the properties of graphite and silicon is given in Table 2.1. It is possible to achieve metal-like conductivity by doping the diamond, commonly used doping atoms are phosphorus and boron. The addition of phosphorus contributes free electrons, whereas the addition of boron creates electron holes in the valence band of an atom. Boron can be incorporated into the diamond lattice quite easily. N-type dopants like phosphorus are much harder to incorporate in the diamond lattice, because these atoms are much larger than boron atoms.

Table 2.1: Properties of CVD diamond, graphite and silicon [4, 5, 6, 7]

Properties	**CVD diamond**	**Graphite crystals (in basal plane)**	**Graphite crystals (across basal plane)**	**Silicon**
Density in g/cm^3	3.52	2.25	2.25	2.33
Young's modulus in *GPa*	1050	1020	36.5	169 in <110> direction
Hardness in *GPa*	100	96	34	13
Thermal conductivity in $W/(m \cdot K)$	2000	2000	10	148
Thermal expansion coefficient in K^{-1}	$1.1 \cdot 10^{-6}$	$0.5 \cdot 10^{-6}$	$27 \cdot 10^{-6}$	$2.6 \cdot 10^{-6}$

Diamond is useful for many different kind of applications[3]. A short list of applications with the properties of diamond that are linked to these applications is shown here:

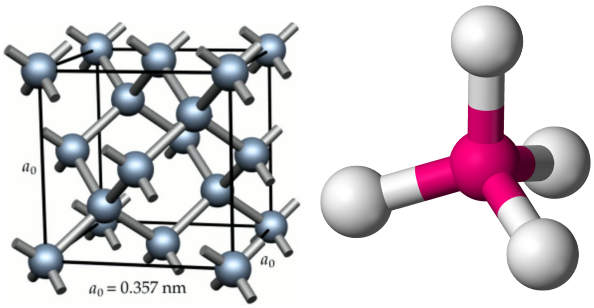

(a) (b)

Figure 2.1: Diamond configurations. a) A unit cell of diamond reprinted from [8], b) tetrahedral configuration

- Cutting tools (extreme hardness and high wear resistance)
- Optical components (high transparency and its high resistance to thermal shock)
- Electronic devices (doped diamond to change it from an electrical insulator to a semiconductor)
- Electrochemical sensors (very large potential window and metallic conductivity), as will be discussed in Paragraph 2.2
- MEMS (high stiffness and high wear resistance)

2.1.2. Diamond synthesis

Figure 2.2 shows the phase diagram of carbon. Graphite is the most stable form of carbon at room temperature and atmospheric pressure. Under these conditions, diamond is only metastable. Because of the energy barrier, the transformation from diamond to graphite does not go spontaneously to the lower energy state (i.e., does not spontaneously turn into graphite)[9]. The material is kinetically rather than thermodynamically stable during growth by chemical vapour deposition.

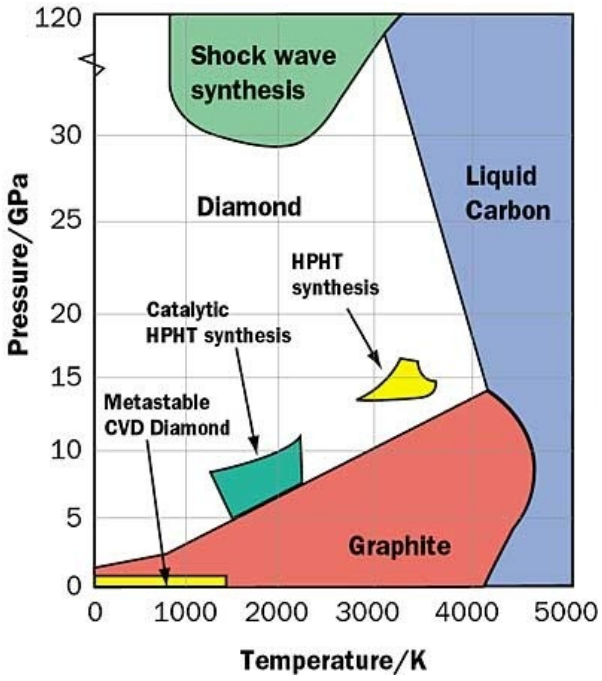

Figure 2.2: Phase diagram of carbon with the different diamond synthesis regimes indicated, reprinted from [10]

As can be seen in the phase diagram, high pressure and temperature are needed to form diamond from graphite. These extreme conditions occur in limited zones of Earth's mantle about 150 kilometres below the

surface where temperatures are at least 1050 degrees Celsius. Diamonds naturally formed in these zones are delivered to Earth's surface during deep-source volcanic eruptions[11].

Synthetic diamonds are commonly produced by two different approaches. The first of them is the so-called "High-Pressure High-Temperature (HPHT)" method, which was established by ASEA in Sweden for the first time [12]. In HPHT synthesis, the extreme pressure and temperature conditions are recreated to produce diamond single crystals from graphite. The second technique is chemical vapour deposition (CVD), a commonly used method for growing polycrystalline diamond thin films. Contrary to HPHT, it is based on low-pressure synthesis of diamond. Figure 2.2 shows also the regimes for HPHT and CVD in the phase diagram of carbon.

Methane, CH_4 (heavily diluted in hydrogen), is often chosen as the main precursor gas and acts as the supplier of carbon atoms. Hydrogen, H_2, is the key element of the process. It drives the chemistry by first breaking the carbon precursors into reactive species, which promote the diamond growth. Hydrogen then opens the bonds on the diamond surface to form new carbon bonds. Finally, it passivates the new atomic layer to stop the atoms from going back into the gas. Hydrogen also removes any non-diamond bond in the diamond layer and prevents the growth of graphite. This process only takes place when the gases are activated[2, 13]. A schematic representation of a CVD process is shown in Figure 2.3[3].

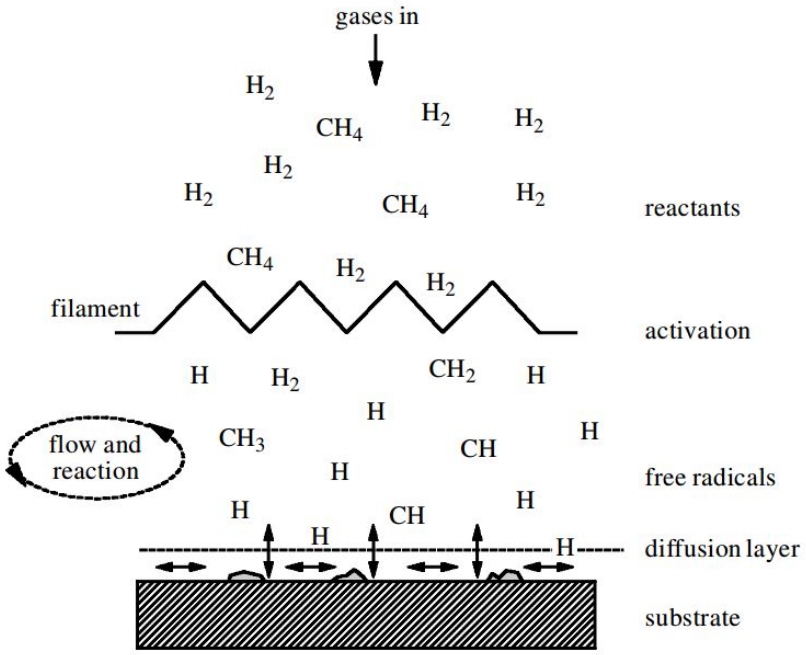

Figure 2.3: Schematic of the physical and chemical processes occurring during diamond CVD, reprinted from [3]

For diamond synthesis, heat or plasma are often used to activate the gases. The CVD processes that make use of those energy sources are hot filament CVD (HFCVD) and microwave-plasma-enhanced CVD (MPCVD). The advantages of HFCVD are that it is a simple process, it is relatively cheap and it is possible to grow large areas (100-400 cm^2). A big disadvantage is the contamination of the diamond film, which is caused by the evaporation of the filament material. Typical growth rates of HVCVD are in the order of max. few microns per hour[3]. The benefits of MPCVD are the great quality of the diamond thin film and the higher growth rate, which can rise to tens of microns per hour[3]. It is possible to use a wide variety of gas mixtures in both techniques, but MPCVD has a slightly broader range of diamond material types that can be synthesised[2]. In Figure 2.4, schematic representation of the set-ups of HFCVD and MPCVD are shown[3].

Diamond can grow on a diamond as well as on a non-diamond substrate, mostly polycrystalline diamond is formed if growth takes place on non-diamond substrates. Polycrystalline means that the film contains many crystals, usually with different orientations and of different sizes[14]. The non-diamond substrate is often pretreated to enhance nucleation kinetics: the substrate is seeded with diamond nanoparticles[13]. The seeding can be done by abrasion, polishing the surface with a diamond grit[3], by dissolving diamond nanoparticles in a solution and dispersing them by means of ultrasonication or by spin coating[15]. During the CVD process, the diamond layer starts to grow from the seeds until individual crystallites touch each other

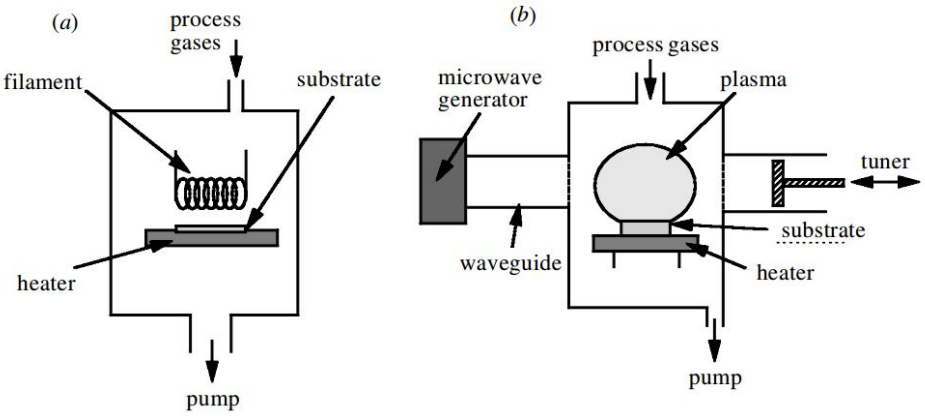

Figure 2.4: a) Set-up of HFCVD, b) set-up of MPCVD. Both reprinted from [3]

(i.e. coalesce) and merge together. A thin layer of polycrystalline diamond is thus formed.
Different morphologies and forms of diamond can be obtained with HFCVD by varying the ratio between hydrogen, methane, argon and nitrogen precursor gases: microcrystalline (MCD), nanocrystalline (NCD), and ultrananocrystalline diamond (UNCD)[16]. An MCD structure has a grain size in the order of one micrometre, NCD has a grain size between six and a few hundred nanometres and the UNCD grain size is between three and seven nanometres. Scanning electron microscope (SEM) images of these morphologies are shown in Figure 2.5[17].

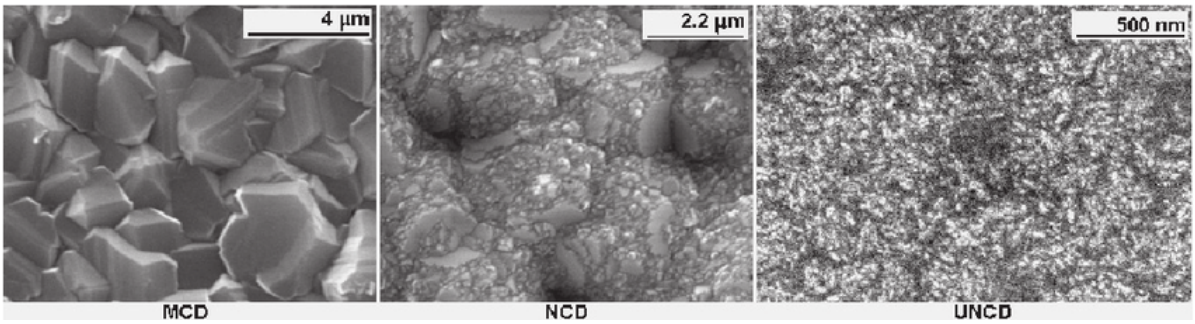

Figure 2.5: SEM images of MCD, NCD and UNCD grown with volume percentages Ar:CH_4:H_2 of 0:1:99, 75:0.5:24.5 and 90:1:9, reprinted from [17]

MCD and NCD can be obtained in hydrogen-rich environments. By increasing the amount of methane, the size of the crystals decreases and NCD can be formed[3]. Both MCD and NCD grow in the same columnar fashion, as can be seen in Figures 2.6 and 2.7. The difference between MCD and NCD is that NCD films are usually thinner and contain smaller grains, which is achieved by increasing the concentration of the diamond seeds during pretreatment[18].

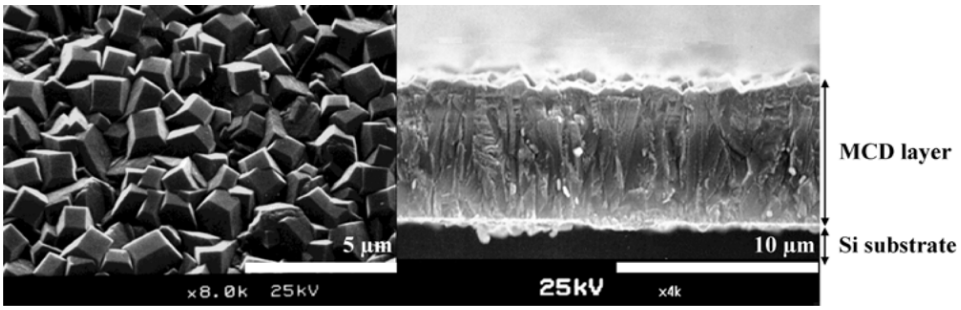

Figure 2.6: Top view and cross-section of a microcrystalline diamond layer (MCD), reprinted from [18]

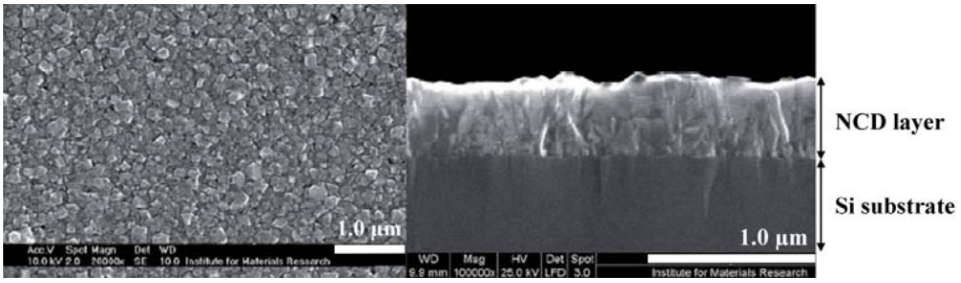

Figure 2.7: Top view and cross-section of a nanocrystalline diamond layer (NCD), reprinted from [18]

By increasing the amount of argon (and decreasing the amount of hydrogen), UNCD structures can be produced[3]. During the synthesis of UNCD there is strong re-nucleation and as a result the grain sizes become even smaller and a more homogeneous layer is formed, see Figure 2.8. Other advantages of UNCD formation are the lower film stress and the improved fracture resistance.

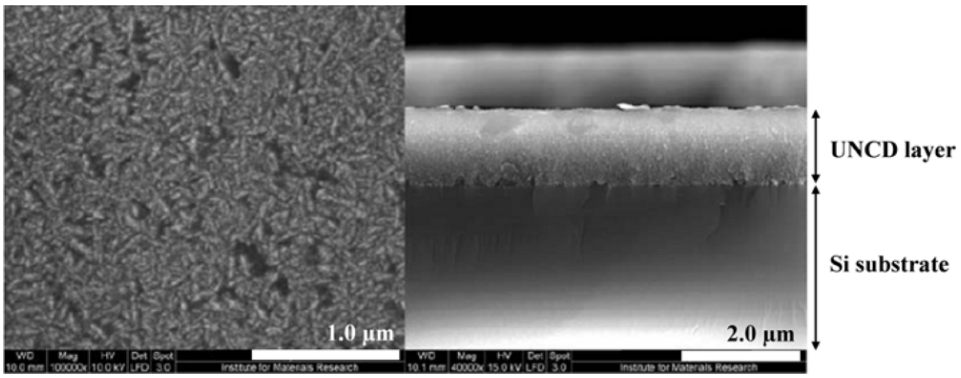

Figure 2.8: Top view and cross-section of an ultrananocrystalline diamond layer (UNCD), reprinted from [18]

2.2. Diamond electrodes

Electrochemical sensing is a powerful technique that is often used these days. These kind of sensors were used for the first time for oxygen monitoring in the fifties. Later, it was also possible to detect different toxic gases. Sensitivity, selectivity and life-time are important properties of these sensors. Diamond is considered to be superior as a material for electrodes because of its outstanding electrochemical properties, like its wide potential window, its very low background current, its high resistance to corrosion, its biocompatibility, and its high resistance to fouling. Diamond is not conductive from itself, it needs to be doped before it can be used as an electrode. Another important thing is the possibility to change the electronic and chemical properties of the electrode by functionalising the surface.

When the first studies were initiated towards the use of diamond electrodes, a lot of research was focused on the effects of different dopant types and concentrations, and the influence of crystallographic orientation on the electrode's performance[19]. Initially, only flat diamond electrodes were used. Nowadays, there is an increasing interest for developing micro- and nanostructured diamond electrodes and electrode arrays. It has become more interesting to add surface modifications to the diamond electrodes as well. One of the reasons for the increased interest in adding surface modifications is to increase the effective area of the electrode; chip sizes are decreasing and thereby also the geometric surface areas. The surface area is an important aspect for sensing performance and a decreasing surface area causes lower signals, which can become unfavourable for electrochemical sensors. However, by nanostructuring the electrode's surface, the surface area can be increased which can improve the sensitivity. The properties of diamond can be enhanced and/or extended by this nanostructuring[20]. An example of such a nanostructure is a nanocylinder made of diamond, as shown in Figure 2.9. Another way to improve the electrode performance is by the modification of the surface. With surface modifications, changes are made to the surface's properties which are favourable for the detection of specific target molecules. For instance, phenyl groups can be added to the BDD electrode's surface to increase the sensitivity to DNA[21].

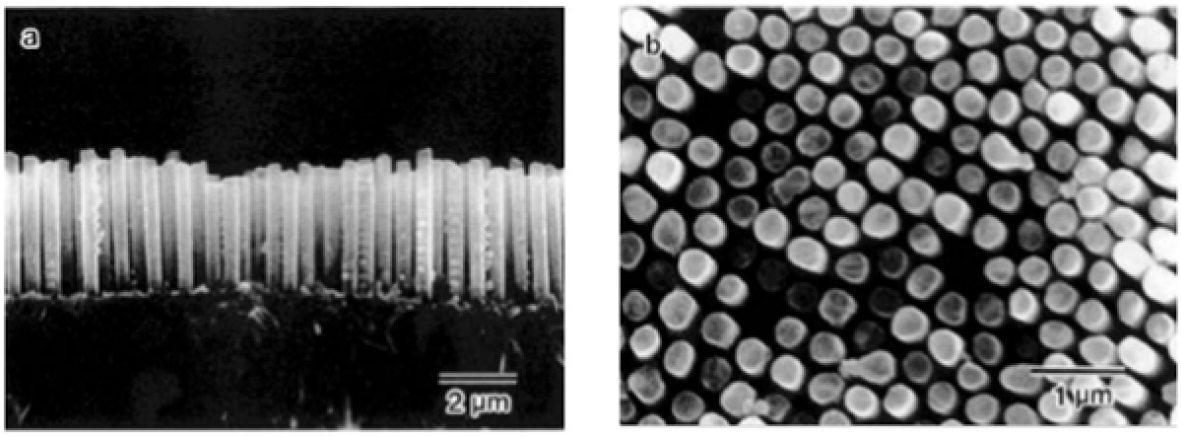

Figure 2.9: Side and top view of well-aligned diamond nanocylinders, reprinted from [22]

2.2.1. Nanostructuring of surfaces

The production methods of diamond nanostructures can be subdivided into two main approaches: bottom-up and top-down approaches[23].

The top-down approach

With the top-down approach you start at the surface of the substrate and etch away material. Often reactive ion etching (RIE) is used for this purpose, which can be done with and without a mask[24]. The density and geometry of the produced diamond nanostructures depend on the initial structure of the diamond thin films and the conditions of the reactive ion etching process[20, 25]. In most cases, a mask is used. Different types of masks can be used, which will be explained next.

Nanoparticles prove to be good etching masks, as high density and uniform diamond nanowires can be obtained. Figure 2.10a shows a schematic representation of the top-down approach using metal nanoparticles as mask for etching. The nanoparticles protect the underlying diamond layer from etching and sputtering. After etching, diamond structures with metal nanoparticles at their tip remain. Figure 2.10b shows a SEM figure of diamond cylinders from a paper of Lee, et al.[20]. The cylinders are made by RIE with oxygen plasma through a two-dimensionally ordered SiO_2 particle array. The diameters achieved are between 0.6-1 μm and lengths are between 3-4 μm. Figure 2.10c shows a SEM figure of vertically aligned diamond nanowires from a paper of Nebel, et al.[26]. Nanowires with lengths between 3-10 nm are obtained using RIE, diamond nanoparticles are used as a mask.

Gold particles are often a good choice, because of the high density and uniform diamond nanostructure arrays that can be achieved[20, 23]. The distribution of gold particles starts with the deposition of a thin layer of gold by means of a sputtering process. After heating at 850 $°C$ in an Ar/H_2-plasma, gold nano-islands with diameters of around 150 nm are uniformly distributed on the surface[20]. Alternatively, diamond nanoparticles are used as a mask, those particles typically have diameters of several nanometres. The diamond nanoparticles are dissolved in water and dispersed on the substrate by ultrasonication. The drawback of using diamond as a material for the nanoparticles is that the nanowires achieved are not that long, around ten nanometres[26].

The deposition of a mask can also be done by making use of electron beam lithography (EBL). An electron-sensitive film (resist), in this case hydrogen silsesquioxane (HSQ), is deposited on a substrate and a focused beam of electrons is used to pattern the resist. The solubility of the resist then changes and makes selective removal possible. A big advantage of using HSQ as a mask is the well-defined positions of the diamond nanostructures that can be achieved[27]. After EBL, the nanostructures are created with RIE. Following, the resist is dissolved. EBL is favourable compared to photolithography for small areas, because of the higher resolution that can be achieved. Unfortunately, it is not suitable to use EBL for large areas, because it takes too long to pattern large areas.

The mask-less top-down approach has the advantage of being simple and straightforward. Diamond nanospikes are produced by RIE in an oxygen plasma[23]. There is no mask deposition or template removal involved, as can be seen in Figure 2.11a[23, 25]. Figure 2.11b shows the boron-doped diamond nanograss arrays grown by the group of Boukherroub[28]. The lengths achieved depend on the etching time, lengths

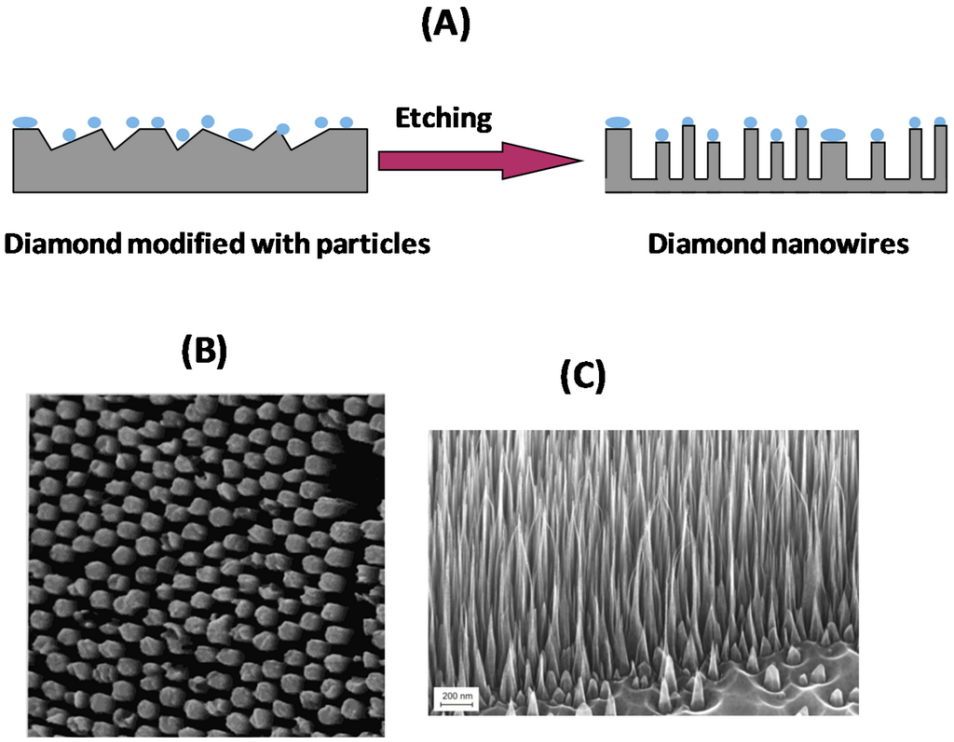

Figure 2.10: All reprinted from [23]. a) Top-down approach with nanoparticles as mask. b)SEM image of diamond cylinders, reprinted from [20]. c) SEM image of vertically aligned diamond nanowires using diamond nanoparticles as masks, reprinted from [26].

between 240-660 nm for etching times between 10-40 minutes are created.

Diamond nanowires with different lengths and diameters and random ordered arrangements can be achieved with the top-down process.

The bottom-up approach

It is possible to grow diamond nanowires by the bottom-up approach by employing a CVD process[24, 23]. It is possible to grow straight diamond nanowires with a uniform diameter and lengths of tens of micrometres by making use of templates that confine the diamond growth[29].

Different kinds of templates can be used. One option is to make use of porous anodised aluminium oxide (AAO) templates. Those templates are often well ordered nano-porous through-hole membranes that contain nucleation sites to grow arrays of polycrystalline diamond nanowires[22]. Such an AAO-template can be placed on top of diamond crystals or is used as seeded, as shown in Figures 2.12 and 2.13. The template can be seeded with ultrasound in a suspension of diamond nanoparticles.
Another type of template is the non-diamond nanowire template (e.g. Si). This template is seeded and a thin diamond layer is deposited on the surface[30].

Diamond nanowires with smaller diameters can be obtained according to the top-down process, which increases the total surface area more than the diamond nanowires grown by means of the bottom-up process. Diamond nanowires have diameters in the order of nanometres and lengths in the range of nanometres to micrometres[31]. The wires have a high surface-to-volume ratio, which is interesting for electrochemical sensing.
The synthesis of diamond nanowires has remained very challenging, as controllability and reproducibility are found to be complicated and hard to manage[15, 31].

2.2.2. Surface functionalisation

It is possible to modify the surface of a flat electrode to achieve better sensing properties. In the case of diamond electrodes this is mostly done by a functionalisation of the surface. Functional groups or non-diamond nanoparticles are added to the surface.

After CVD growth of diamond films, the surface is covered with hydrogen, but for instance oxygen containing functional groups can be attached to the surface as well. It is possible to control or modify the surface

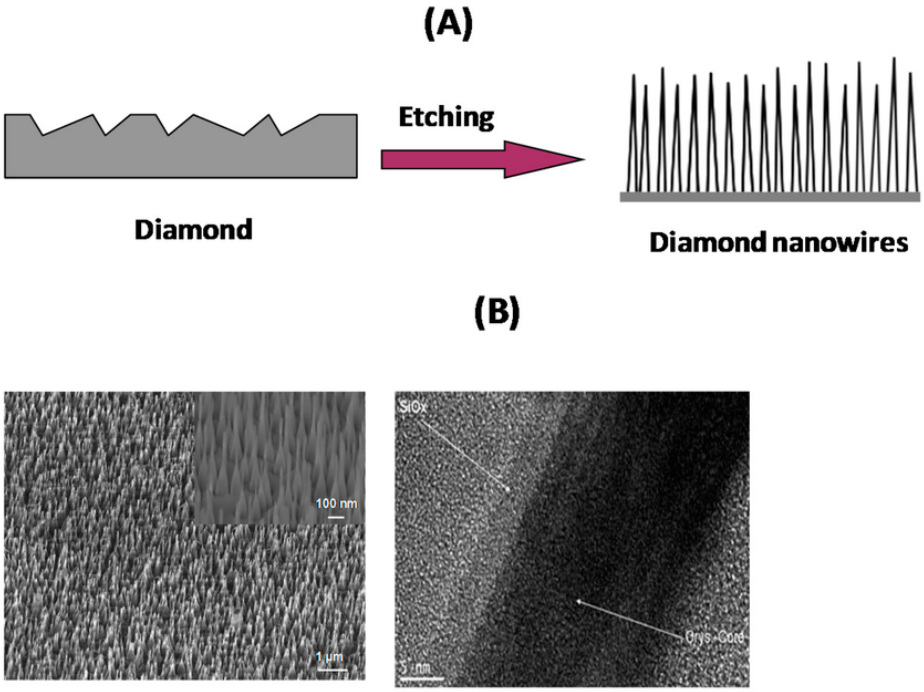

Figure 2.11: All figures reprinted from [23]. a) Top-down approach without a mask, b) and c) SEM and HR-TEM images of boron-doped diamond nanowires synthesized through maskless technique, reprinted from [25]

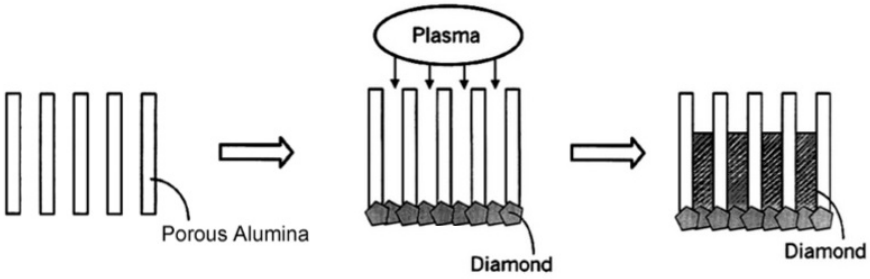

Figure 2.12: Bottom-up approach, reprinted from [24]

properties by adding chemical groups, for instance properties like the roughness, hydrophilicity, and biocompatibility can be changed. For instance, oxygen creates a hydrophilic surface, whereas hydrogen creates a hydrophobic surface. It is also possible to add more complex functionalities which can improve the detection of specific target molecules. For instance, tips of diamond nanowires were electrochemically functionalised with phenyl groups to improve the detection of DNA[32].

Another way of surface functionalisation is the addition of metal nanoparticles. These nanoparticles can work like an electrocatalyst and change the mass transport on an electrode. This can improve the detection of specific target molecules to achieve higher reaction rates. The successful addition of nickel[33], platinum[34], and gold[35] has already been reported in literature.

2.3. Characterisation methods

The characterisation of the different surface modified boron-doped diamond electrodes is done by scanning electron microscopy (SEM), Raman spectroscopy, cyclic voltammetry (CV), and electrochemical impedance spectroscopy (EIS). These methods will be explained in this section.

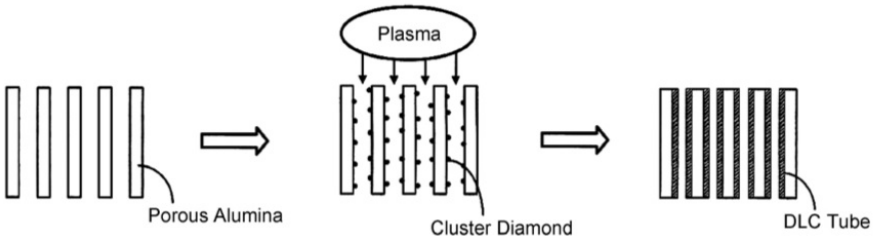

Figure 2.13: Coating of nanowires by seeding, reprinted from [24]

2.3.1. Scanning electron microscopy

A scanning electron microscope scans the surface with a focused beam of electrons, see Figure 2.14a. The electrons, which carry significant amounts of kinetic energy, interact with the atoms in the sample. By the dissipation of the kinetic energy, various signals are produced that contain information about the sample's surface topography and composition. The secondary electrons and backscattered electrons are commonly used for the imaging of a sample. A SEM figure of the surface of a boron-doped diamond film is shown in Figure 2.14b.

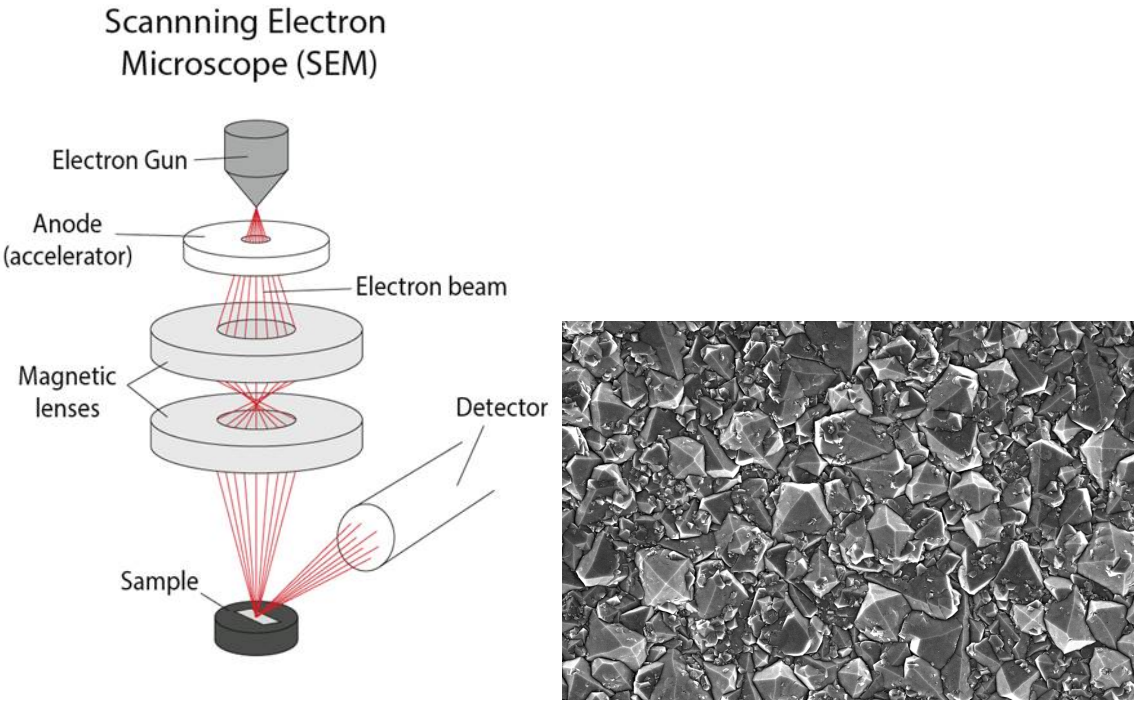

(a) (b)

Figure 2.14: Scanning electron microscopy. a) SEM, b) SEM figure of BDD

2.3.2. Raman spectroscopy

Raman spectroscopy is a spectroscopic technique used to observe vibrational modes and other low-frequency modes in a material, such as a thin-film BDD sample. Raman spectroscopy is commonly used in diamond research, for example, to detect differences in composition (i.e., sp^3/sp^2-C ratio) and stress states of diamond thin-film samples. In a Raman spectroscopy setup, a laser light shines on the sample's surface and is absorbed, transmitted, and backscattered. The backscattered light is guided by filters, lenses, and mirrors to the detector as can be seen in Figure 2.15. The laser light interacts with the molecular vibrations, which causes

an energy shift in the photons. This gives information about the vibrational modes of the system and the specific molecules on the surface.

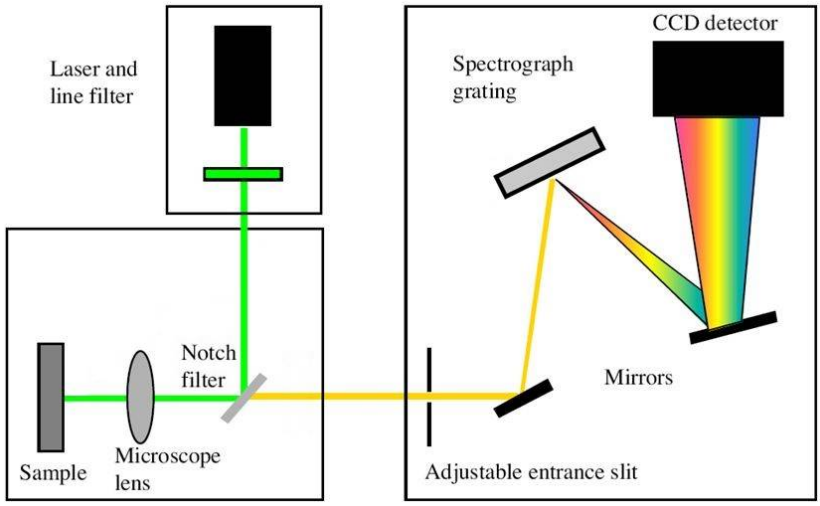

Figure 2.15: Raman spectroscope

2.3.3. Electrochemical characterisation

The electrochemical characterisation of the samples can be done with cyclic voltammetry (CV) and electrochemical impedance spectroscopy (EIS). Information about reversibility and transfer kinetics can be obtained.

Cyclic voltammetry

The electrochemical cell contains three electrodes, an electrolyte and a potentiostat. The three electrodes are the working (WE), counter (CE), and reference electrode (RE). In the used setup those electrodes are made of diamond, platinum, and silver-silver-chloride (Ag/AgCl), respectively. A potentiostat is an electronic instrument that controls the potential between the WE and the RE, while adjusting the current at the CE. The potential and current are continuously monitored and all data is collected in the software program Nova (version 1.10). Cyclic voltammograms are produced with this software, these voltammograms are used to analyse the performance of the WE. Figure 2.16 shows such a plot of current as a function of applied potential in an electrolyte containing redox species. When the electrolyte contains for instance an acidic solution, like nitric acid (HNO_3), the potential window of the diamond electrode can be determined. At this point there are no redox reactions. By adding a redox species, ruhex or ferrocyanide for instance, a redox reaction can occur. Redox peaks, also called peak currents, can be measured.

Two peak currents can be seen. An upwards peak, called the anodic peak or oxidation peak, and a downwards peak, called the cathodic peak or reduction peak. The extrapolated background baselines are drawn in a cyclic voltammogram after the measurements are done. These baselines help to determine the peak current values. The peak current is measured from the peak down to the baseline, as can be seen in Figure 2.16. The formal potential $E^{0'}$ and the peak-to-peak potential ΔE_p are also determined by the cyclic voltammogram. The formal potential is calculated by adding the values of the anodic peak potential and the cathodic peak potential and divide it by 2. The peak-to-peak potential is the value obtained by subtracting the values of the anodic peak potential and the cathodic peak potential.

Higher oxidation and reduction peaks are achieved when higher scan rates are applied. When the peaks are shifting to the sides, the peak on the forward scan to the right and the peak on the backward scan to the left, the transfer rate constant k_0 is decreasing. This means that there is a quasi-reversible or irreversible process. For a reversible process, the peaks would have appear at the same potentials with different scan rates.

The electrochemical reversibility of the electron transfer reaction is related to how fast such a reaction is. A reversible reaction has a fast electron transfer process. Quasi-reversible reactions have an intermediate

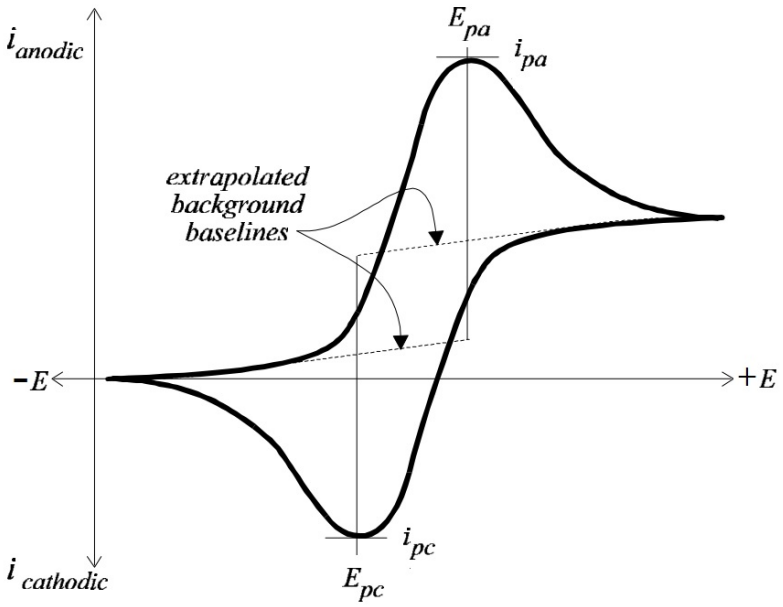

Figure 2.16: Basic cyclic voltammogram reprinted from the manual of Pine Instrument Company

speed electrode reaction and irreversible reactions have a very low electron transfer. To check the reversibility of an electron transfer mechanism, it is needed to check five criteria[36]:

1. Relation between electron transfer rate constant k_0 and mass transport m_{trans}
   - If $k_0 \gg m_{trans}$ the electrode process is reversible and diffusion-controlled
   - If $k_0 \approx m_{trans}$ the electrode process is quasi-reversible
   - If $k_0 \ll m_{trans}$ the electrode process is rate-determined and irreversible
2. Correlation between Nicholson parameter Ψ and electron transfer rate constant k_0
   - The electron transfer mechanism is reversible if $\Psi > 10$ and $k_0 > 0.35 \cdot v^{1/2}$
   - The electron transfer mechanism is quasi-reversible if $10 > \Psi > 10^{-2}$ and $0.35 \cdot v^{1/2} > k_0 > 3.5 \cdot 10^{-4} \cdot v^{1/2}$
   - The electron transfer mechanism is irreversible if $\Psi < 10^{-2}$ and $k_0 < 3.5 \cdot 10^{-4} \cdot v^{1/2}$
3. The process is reversible if the anodic and cathodic peak currents are the same.
4. The process is reversible if the peak current is proportional to the square root of the scan rate, according to Randles-Sevcik equation.
5. The process is reversible if the potential between the anodic and cathodic peak is constant at all scan rates.

To calculate the electron transfer rate constant k_0, Equations 2.1, 2.2 and 2.3 are needed:

$$k_0 = \frac{D_0^{1/2}}{e^{((\Delta E_p - E^{0'}) \cdot \frac{\alpha F}{RT} + 0.78 + 0.5 \cdot ln \frac{\alpha F v}{RT})}}, \tag{2.1}$$

$$D_0 = \frac{b}{2.99 \cdot 10^5 C n^{3/2} \alpha^{1/2}}, \tag{2.2}$$

$$\alpha = \frac{1.857RT}{F|\Delta E_p - E_{p/2}|}, \tag{2.3}$$

where D_0 is the diffusion coefficient of oxidised species in m^2/s, ΔE_p is the potential difference between the anodic and cathodic peak in V, $E^{0'}$ is the formal potential in V, α is the transfer coefficient, F is the Faraday constant which is 96485.33 C/mol, R is the gas constant which is 8.314 $J/(molK)$, T is the temperature in K, v is the scan rate in V/s, b is the slope of the graph with current in A/m^2 versus the square root of the scan rate in $\sqrt{\frac{V}{s}}$, C is the bulk concentration in mol/m^3, n is the number of electrons transferred and $E_{p/2}$ is the half-peak potential in V.

The mass transport can be calculated with equation 2.4

$$m_{trans} = \sqrt{\frac{\pi nFD_0 v}{RT}} \tag{2.4}$$

The Randles-Sevcik equation gives the relation between the current in A/m^2 and the square root of the scan rate in $\sqrt{\frac{V}{s}}$, as can be seen in Equation 2.5, where i_p is the peak current in A and A is the exposed surface area in m^2.

$$i_p = 0.4463 \frac{n^{3/2}F^{3/2}}{\sqrt{RT}} AD_0^{1/2} C v^{1/2} \tag{2.5}$$

The drawback of this formula is that it is only valid for reversible electrode processes. For irreversible or quasi-reversible processes, the equation of Nicholson and Shain (Equation 2.6) can be used [37].

$$i_p = (2.99 \cdot 10^5) n^{3/2} \alpha^{1/2} AD_0^{1/2} C v^{1/2} \tag{2.6}$$

Another way to determine the electron transfer rate constant k_0 is by making use of Nicholson's method [38]. Nicholson makes use of a dimensionless kinetic parameter Ψ:

$$\Psi = \frac{(D_0/D_R)^{\alpha/2} k_0}{(\pi D_0 vF/RT)^{1/2}}, \tag{2.7}$$

where D_R is the diffusion coefficient of reduced species in m^2/s. When the transfer coefficient α is within 0.3 and 0.7, the peak-to-peak potential difference ΔE_p is independent of α. Besides, both diffusion coefficients are almost similar, which means that we can assume that $\frac{D_0}{D_R} = \approx 1$. This makes it a lot easier to calculate k_0. It is possible to found the value of Ψ by a table. In Table 2.2 the values of the dimensionless kinetic parameter Ψ versus the potential difference between the anodic and cathodic peak ΔE_p are shown[38].

Table 2.2: Reprinted table with values for the kinetic parameter and the peak-to-peak potential difference for CV[38]

Ψ	ΔE_p in mV
20	61
7	63
6	64
5	65
4	66
3	68
2	72
1	84
0.75	92
0.5	105
0.35	121
0.25	141
0.1	212

Electrochemical impedance spectroscopy

A small sinusoidal potential is applied at a fixed frequency. The response is measured and the impedance at this frequency is computed. The electrochemical impedance can be measured at a range of frequencies. Plots

of the results can be made by a program, Nova for instance, and can be analysed. The impedance data are often shown as a Bode plot or a Nyquist plot. A bode plot is a plot with separated graphs for the magnitude and the phase of the response. A Nyquist plot is a plot in the complex plane, the magnitude and phase are the directory of this plot. Each point in a Nyquist plot shows the impedance at one frequency. Electrochemical cells can be modelled as an electrical circuit. Such a circuit consists of components like resistors (R) and capacitors (C). This circuit represents the electrochemical behaviour of the diamond electrode. The electrochemical impedance is the response of the electrochemical cell to an applied potential. Possible properties that result from fitting of the EIS measurement can be the charge-transfer resistance, the diffusion coefficient and the electron transfer rate.

By an EIS fitting program an equivalent circuit can be chosen to achieve the best fitting. One of the simplest possible models describing processes at the electrochemical interface is the Randles circuit, Figure 2.17 shows the Nyquist plot and the circuit diagram of a simple Randles circuit[39]. The Randles circuit contains two resistors, the active electrolyte resistance R_S and an active charge transfer resistance R_{CT}, a capacitor C_{dl} that represents the double layer and the Warburg element W, which is a diffusion element representing the diffusion of redox species towards the electrode. The capacitor C_{dl} is often replaced to a constant phase element CPE. A CPE is an equivalent electrical circuit component that models the behaviour of a double layer, it is an imperfect capacitor. The graph shows also the areas of kinetic and mass transfer (diffusion) control. The semi-circle declares the kinetics region. Larger semi-circles mean larger transfer resistance values. This can be due to lower doping levels, which causes a lower conductivity of the sample. The straight line declares the diffusion region, the phase between the semi-circle and the straight line is 45 degrees for infinite Warburg diffusion. The diffusion region can be modelled with a Warburg impedance. This impedance represents the resistance to mass transfer and has a low frequency character. The diffusion coefficient can be calculated by making use of the EIS-plot and the Warburg formula. The Warburg formula is:

$$W = \frac{\pi\sqrt{2}}{nFA\sqrt{D}C^*}, \tag{2.8}$$

where W is the Warburg constant in $\Omega \cdot s^{-1/2}$, n is the number of electrons transferred per mole of product, F is the Faraday constant in C/mol, A the exposed surface area in cm^2, D is the diffusion coefficient in cm^2/s and C^* the concentration in mol/cm^3.

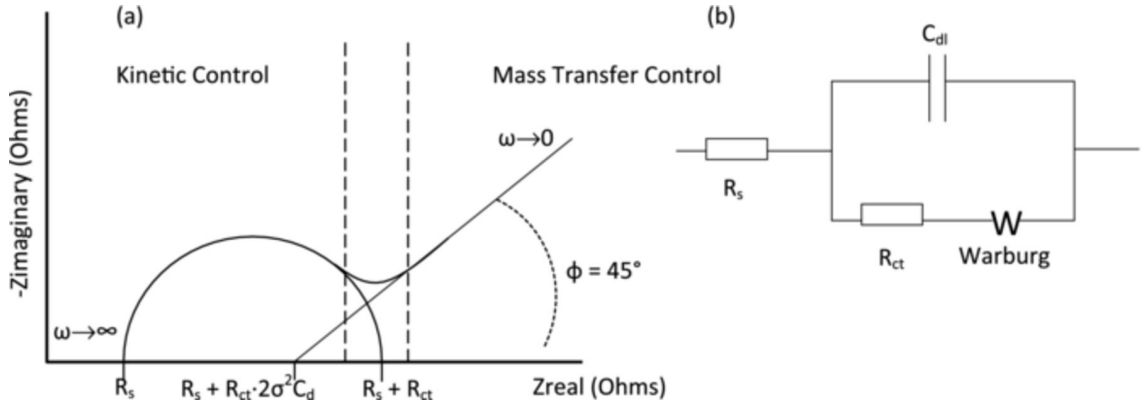

Figure 2.17: Randles circuit with its' corresponding a) Nyquist plot, and b) circuit diagram. Both reprinted from [39]

The transfer rate constants can also be calculated when the active charge transfer resistance R_{CT} is known. The following formula can be used:

$$k_0 = \frac{RT}{n^2F^2A(C_O)^{\alpha}(C_R)^{1-\alpha}R_{CT}} \tag{2.9}$$

The concentrations of the oxidation and reduction species, C_O and C_R, are equal when the system is in equilibrium.

2.4. Electrolytes

The potential window and the background current of a diamond electrode can be determined by having a look at cyclic voltamogramms where for instance acids is used as an electrolyte. Acids like nitric acid (HNO_3)

and sulphuric acid (H_2SO_4) are often used in literature to determine the potential window of a diamond electrode.

For the electrochemical characterisation of diamond, ruhex ($Ru(NH_3)_6^{3-}$) and ferrocyanide ($Fe(CN)_6^{4-}$) are often used as redox mediators. The redox reactions of these two mediators are shown below:

$Ru(NH_3)_6^{3-} \rightleftharpoons Ru(NH_3)_6^{2-} + e^-$

$Fe(CN)_6^{4-} \rightleftharpoons Fe(CN)_6^{3-} + e^-$

With a redox reaction, an oxidation and reduction reaction can take place. There is a loss or a gain of electrons. When ferrocyanide oxidises this results in ferricyanide, which means that there is a loss of an electron. In Figure 2.18 cyclic voltammograms of BDD in ferrocyanide and ruhex are shown[40]. At the upward peaks there is a loss of an electron (oxidation) and at the downward peaks there is a gain of an electron (reduction).

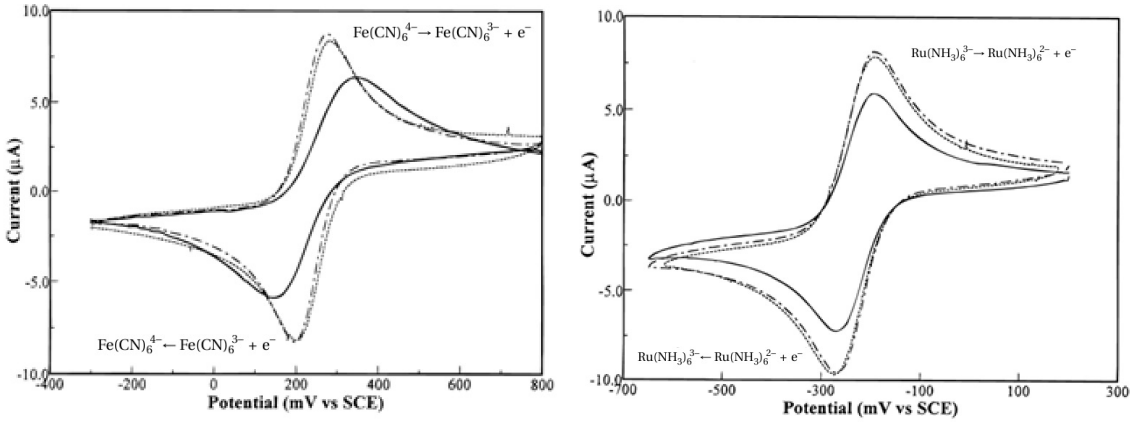

(a) (b)

Figure 2.18: Cyclic voltammograms of different pretreated BDD electrodes in the redox mediators a) ferrocyanide, and b) ruhex. Reprinted from [40]

The biggest difference between ferrocyanide and ruhex has to do with how the electron transfer takes place, this can be outer-sphere or inner-sphere. Ruhex undergoes an outer-sphere electron transfer, while ferrocyanide undergoes as inner-sphere electron transfer. With the outer-sphere reaction electron transfer takes place at the outer Helmholtz plane, this plane passes through the centres of solvated ions at the distance of their closest approach to the electrode. The outer Helmholtz plane is also called electrical double layer[41]. Electron transfer takes place from one primary bond system to another one. This kind of transfer is relatively insensitive to the surface termination and the microstructure of the surface. For an inner-sphere redox reaction, the electron transfer takes place through the ligand adsorbed on the electrode's surface. This ligand lies in the inner Helmholtz plane, this plane passes through the centres of the specifically adsorbed ions[41]. The electron transfer takes place within a primary bond system where the ions share a ligand. The rate constant is highly dependent on the electrode material. The species require a strong interaction with the electrode's surface in order to exchange electrons[42].

2.5. Glucose sensors

Worldwide 2.8 percent of the population suffered from diabetes in 2008 [43]. It is the most consistent chronic disease in the Netherlands. There are two types of diabetes. People with diabetes type 1 do not produce any insulin, while people with diabetes type 2 produce too much or too less insulin. Insulin is a hormone that is needed to manage the blood sugar level. Glucose sensors are used to measure the blood sugar level.

There are two types of glucose sensors: non-enzymatic and enzymatic sensors. Non-enzymatic glucose sensors can directly detect glucose, while enzymatic glucose sensors detect the glucose indirectly. By direct glucose sensing the glucose oxidises at the electrode's surface[44]. The enzyme glucose 1-oxidase (GOx) is used mostly these days for indirect glucose sensing. GOx oxidises the glucose and produces hydrogen peroxide, this hydrogen peroxide is measured by the sensor to (indirectly) determine the amount of glucose[45]. Advantages of GOx are the high selectivity, high sensitivity and good stability compared to other enzymes. A big disadvantage of the enzymatic sensors is the instability of enzymes. Those enzymes, like GOx, are affected by ambient conditions like temperature, oxygen, humidity and acidity. Furthermore, complicated production

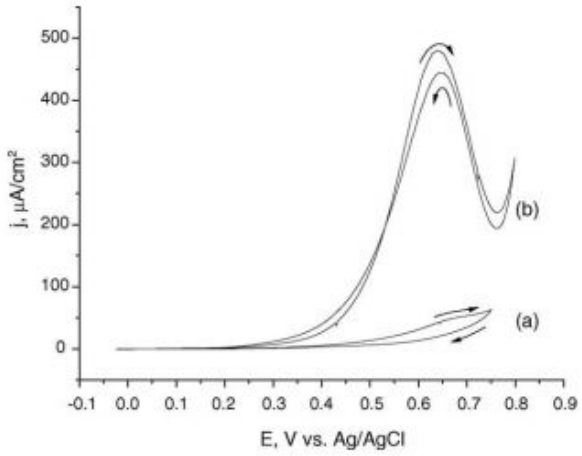

Figure 2.19: CVs with 5 mM glucose at: a) diamond electrodes after severe anodic polarization, and b) hydrogen flame annealed diamond electrodes. The supporting electrolyte was 1 M NaOH and the scan rate was 20 mV/s. Reprinted from [45]

processes are needed to make the immobilization of the enzymes possible. The advantages of non-enzymatic sensors are that it is stable, simple and has low production costs. However, adsorbed oxidised products on the surface can cause a decrease in activity and poison the electrode, this is also called fouling[44]. A few papers state that they were able to detect glucose with bare unmodified BDD[30, 44, 45]. A paper by S. Park, et al. reported that a hydrogen flame pretreatment was used to remove the oxygen functionalities on the surface. The paper says: "It seems the annealing process increases the surface conductivity of the electrode by removing the oxygen functionalities at the electrode surface. XPS spectra indicate that O 1s levels decreased by 21 percent after annealing with hydrogen flame"[45]. Figure 2.19 shows a CV in glucose with bare BDD after anodic polarisation (a) and after hydrogen flame treatment (b). There is a big difference in response, the sample that was treated by the hydrogen flame has a much higher peak at 650 mV than the anodic polarised sample.

Zhao et al. measured glucose on microcrystalline and nanocrystalline BDD at scan rates up to 50 mV/s[44]. At higher scan rates the response was hardly seen, this can be due to slow desorption kinetics. The active sites are not relinquished on time to adsorb new oxidation products during the new oxidation step.

Luo et al. used a bare and a structured BDD sensor[30]. The sensor was structured with nanorods, in the paper called a nanoforest. Figure 2.20 shows a SEM figure of the BDD nanoforest and a positive potential scan in 0.1 M NaOH solution containing 0.1 mM glucose for both BDD and BDD nanoforest samples. In the paper is mentioned that the faradaic currents for glucose oxidation strongly depend on the surface structure of the electrode[30].

There are also papers that report that it is not possible to measure glucose with bare BDD.

Modifications of the BDD surface with metal nanoparticles like gold, platinum, copper[46] and nickel[47, 48] have been researched. These nanoparticles can be used as catalysts to achieve a better detection of glucose. The sensitivity that can be achieved with these metal particle-modified electrodes is much higher than with bare BDD, 101.9 $\mu AmM^{-1}cm^{-2}$ and 8.1 $\mu AmM^{-1}cm^{-2}$, respectively.

An overview of some non-enzymatic glucose sensors made of BDD is shown in table 2.3.

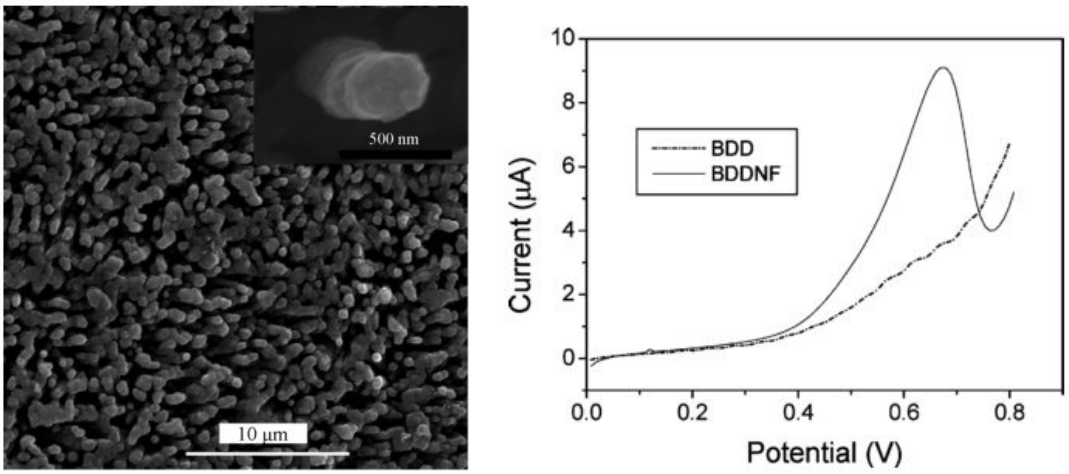

(a) (b)

Figure 2.20: a) SEM image of BDD nanorod forest, and b) CV in 0.1 M NaOH containing 0.1 mM glucose. Both reprinted from [30]

Table 2.3: Non-enzymatic glucose sensors made of BDD

Comp.	Pretreatment	Sens. in $\mu A/mMcm^2$	Lin. range in mM	LOD in μM	Year	Ref.
Ni-BDD	-	2.8	0.001-0.05	0.67	2004	[49]
Cu-BDD	-	6.4	0.001-0.05	1.50	2004	[49]
BDD	Immersed in hot aqua regia for 30 min, rinsed with deionized water, immersed in warm H_2O_2 for 30 min, rinsed with deionized water, annealed with hydrogen flame for 10 min.	-	0.5-10	500	2005	[45]
Cu-BDD	-	9.2	1-5	-	2006	[46]
BDD, NCD	Sonicated in isopropanol, acetone and ultrapure water for 15 min, respectively, and dried under a nitrogen stream	101.9	0.25–10	25	2009	[44]
BDD nano-forest	Washed under ultrasonication in 2-propanol followed by ultrapure water for 10 minutes	8.1	0-7	0.2 ± 0.01	2009	[30]
Ni-BDD	-	-	-	-	2009	[48]
Ni-BDD	Cleaned using a diamond slurry, sonication for 1 min in ethanol/water, rinsing using deionised water	1040	0.005-10	2.7	2010	[47]
BDD + NWs	-	49.34	0.06-8	60	2013	[50]
Pt/Au-BDD	-	1.70	0.01-7.5	7.7	2017	[51]

3

Research focus

Diamond is an excellent material with great electrochemical properties. It has a wide potential window, high resistance to fouling and corrosion, high electric conductivity when doped with boron, it is biocompatible and it has a very low background current. These properties make diamond an excellent choice for electrodes for electrochemical sensing. Electrochemical sensing is a simple and fast way to detect and measure (bio)molecules accurately in fluids.

Nowadays, there is a new trend leading to electrodes getting smaller. One of the current challenges in the development of diamond micro-electrodes and micro-electrode arrays is to increase the sensitivity of the diamond electrodes, while the electrode's dimensions decrease.

The effective surface area of an electrode can be increased by the nanostructuring of the surface. With nanostructuring, structures are created on the diamond's surface. Another way of improving the sensitivity of an electrode is by the functionalisation of the surface. Functional chemical groups, for instance containing hydrogen or oxygen, can be added to change the surface properties and possibly thereby increasing the sensitivity for specific target molecules. Another way of surface functionalisation is the addition of metal nanoparticles. These particles can work like an electrocatalyst and change the mass transport on an electrode.

An interesting biomolecule to detect is glucose. 2.8% of the world population suffers from diabetes, these people need to measure their blood sugar level and manage this level by dispensing insulin in their body when needed. A glucose sensor is used to determine the amount of glucose in the blood. BDD is an interesting material for the non-enzymatic detection of glucose. Some research has already been done on non-enzymatic glucose sensing with BDD electrodes. However, contradicted conclusions have been reported about sensing glucose on flat BDD electrodes. This means that it is still interesting to research this field.

The goal of this thesis is to electrochemically characterise nanostructured and surface-modified boron-doped diamond (BDD) electrodes and see which sensitivities for non-enzymatic glucose sensing can be achieved. Comparison will be made with as-grown, bulk BDD electrodes. The characterisation of the BDD electrodes will be done by scanning electron microscopy, raman spectroscopy, cyclic voltammetry, and electric impedance spectroscopy.

Research in the field of the electrochemical sensing of (bio)molecules with BDD electrodes is completely new for the diamond group of PME. Own methods and techniques need to be evaluated and a standard characterisation protocol need to be made. It is researched if it is possible to achieve the same, or even better, results as from literature.

4

Experimental work

First, the samples were prepared, terminated, structured, and characterised, which is described in Section 4.1. The procedures, equipment, and chemicals that are used during the electrochemical measurements are described in Section 4.2.

4.1. BDD samples

4.1.1. Preparation of samples

An 8-inch silicon wafer with a 4 μm thick film of B-NCD is grown by IMEC. Prior to CVD diamond growth, a Si (100) wafer substrate with a diameter of 200 mm was spin-seeded with 5 nm sized diamond nanoparticles (NanoAmando aqueous colloid, NanoCarbon Research Institute). A seeding density of about 5x10^{10} cm^{-2} was established. The seeded wafers were then transferred to a hot filament chemical vapour deposition (HFCVD) reactor (sp^3 Diamond Technologies, model 655), and the diamond film was grown using a three-gas chemistry of hydrogen (H_2), methane (CH_4), and trimethylborane (TMB). The CH_4/H_2 gas ratio was set at 2.4 % (72 $sccm$/3000 $sccm$) and the pressure at 8 $mbar$, resulting in NCD films. The substrate temperature was about 1123.15 K during growth. The TMB flow was kept at 40 $sccm$ to attain the highest, metallic conductivity (5x10^{-3} cm). SEM figures of the as-grown BDD are shown in Figure 4.1.

4.1.2. Surface termination and structuring of the electrodes

The wafer that was grown by IMEC, as described in Section 4.1.1, is cut into smaller pieces and used during all measurements. During this thesis five different electrodes are used, these are listed in Table 4.1.

Electrodes 2, 3 and 4 are made from the bare BDD sample. First, this bare BDD is acid cleaned in boiling concentrated HCl + H_2SO_4 + HNO_3 until the colour of the solution became transparent. A gold layer with a thickness of 5 nm is deposited with electron-beam evaporation (Leybold L560 in Kavli Nanolab Delft). The

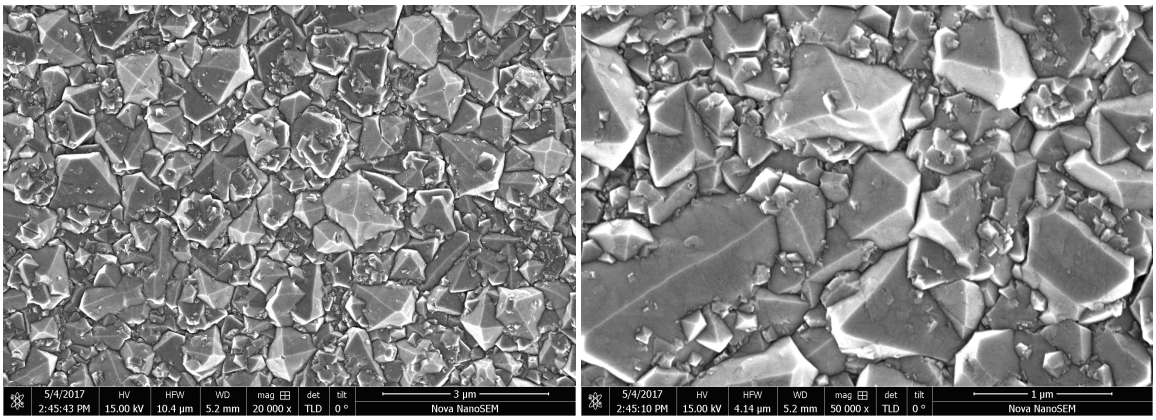

Figure 4.1: High resolution SEM figures of as-grown BDD

Table 4.1: All used electrodes

Sample number	Sample description	Abbreviation
1a	as-grown BDD	BDD
1b	acid cleaned BDD	BDD-acid
2	BDD with gold nano-islands	BDD+gold
3	BDD with diamond nanowires	BDD+NWs
4	BDD with diamond nanowires and gold on top of the wires	BDD+NWs+gold

deposition rate that was used is 0.3 Å/s. The gold nano-islands are made by a dewetting process in the HFCVD tool with a temperature between 1073.15 K and 1123.15 K for seven minutes under argon flow (200 $sccm$). The pressure used is around 2-3 $mbar$. SEM figures of the deposited gold layer before and after dewetting are shown in Figure 4.2. Electrode 2 is made of BDD with dewetted gold nanoparticles on top of it.

The nanowires with gold on top of the wires are produced by the reactive ion etching of electrode 2 (Alcatel GIR-300 in Kavli Nanolab Delft). An oxygen flow of 50 $sccm$, a pressure of 30 μbar and a 100 W RF power are used. Electrode 4 is a BDD with diamond nanowires and gold particles on top of these wires that is etched for 4 minutes, this can be seen in Figure 4.3. To achieve electrode 3, BDD sample with diamond nanowires and without gold particles, electrode 4 is acid cleaned until all gold is removed.

4.1.3. Film characterisation

The characterisation of the different surface modified boron-doped diamond electrodes was done by scanning electron microscopy (SEM) and Raman spectroscopy. The working principles of these methods are described in section 2.3.

Scanning Electron Microscopy

The SEM figures of as-grown BDD can be seen in Figure 4.1. The SEM figures of the deposited and dewetted gold and of the nanowires with gold are made at TU Delft at the Kavli Nanolab Delft on the FEI NovaNanoSEM. These SEM figures are shown in Figures 4.2 and 4.3.

Raman spectroscopy

Raman measurements were done at TU Delft at the faculty 3mE in the optical lab using a Horiba Scientific Raman Spectroscope. The Raman spectrum of the as-grown BDD sample is shown in Figure 4.4 The bands related to boron-doped diamond are clearly visible in this spectrum. The B-related band, D-band and G-band can be seen. The G-band is related to graphite (sp^2-carbon), the D-band is related to disordered carbon and the B-band is related to the boron-doping level[52].

4.2. Electrochemical measurements

4.2.1. Set-up

A new dedicated electrochemical cell was designed and constructed to perform the electrochemical experiments. The most important aspect of the new set-up is the controlled exposed surface area of the diamond electrode. The new set-up is shown in Figure 4.5. The beaker is made of Teflon and printed by a 3D-printer. The total length from the top of the beaker to the bottom of the sample holder is 13 cm.

The diamond electrode (working electrode) is pressed between a rubber O-ring and a connecting copper plate. The backside of the diamond electrode is made of silicon, which is not conductive. Silver paste is used to complete the circuit between the diamond surface and the copper plate. The area that is exposed to the electrolyte is 0.218 cm^2. The platinum electrode (counter electrode) and Ag/AgCl electrode (reference electrode) were mounted in the Teflon beaker. The platinum and Ag/AgCl electrode are both purchased from BAS Inc.. The platinum wire has a length of 5.7 cm and has cat.no. 002222. The Ag/AgCl electrode's cat.no. is 012167.

4.2.2. Cleaning process

It is important to clean the electrodes before usage to make sure that there are no impurities on the surfaces which can cause unwanted anodic and cathodic peaks during cyclic voltammetry measurements. The bare

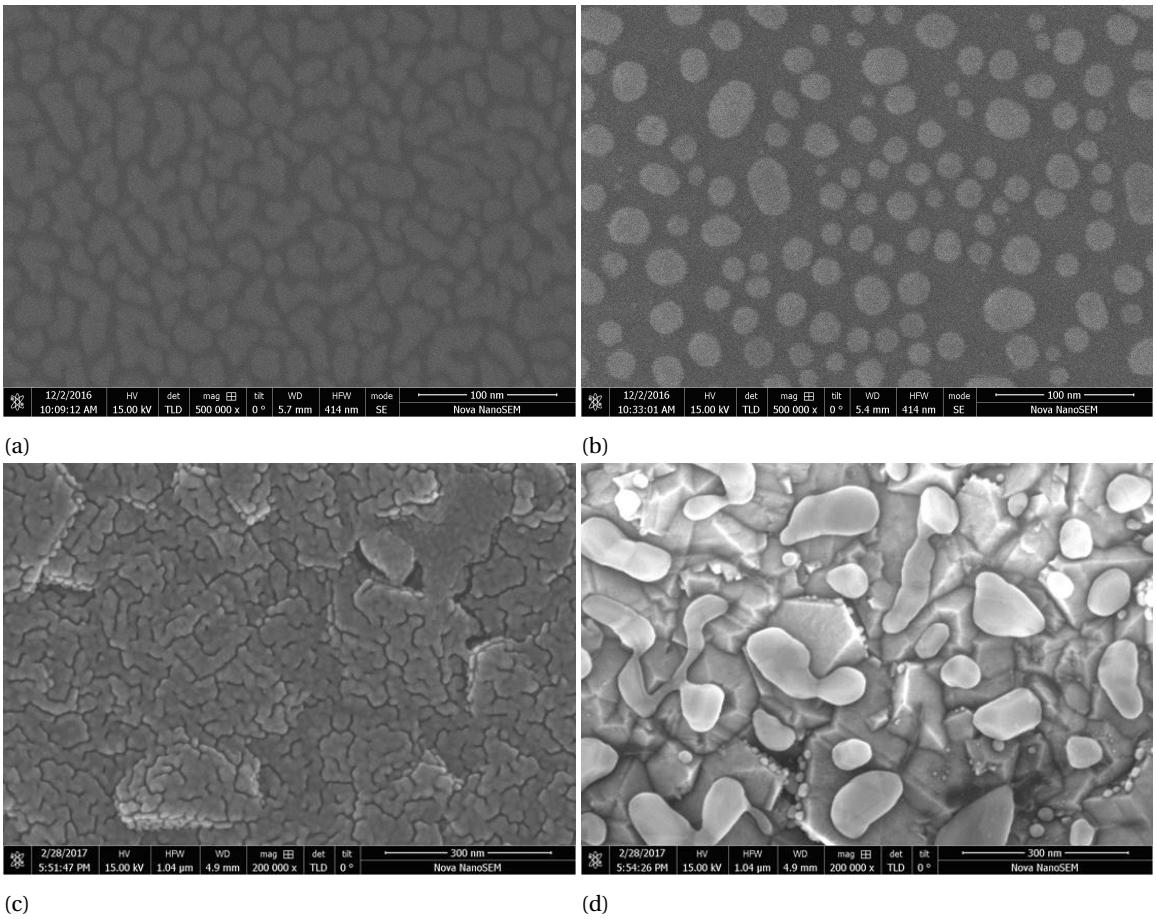

(a) (b)

(c) (d)

Figure 4.2: SEM figures of the BDD with gold. a) and c) show the gold layer before the dewetting. b) and d) show the gold nanoparticle islands after dewetting. Figures c) and d) are made by a high resolution SEM

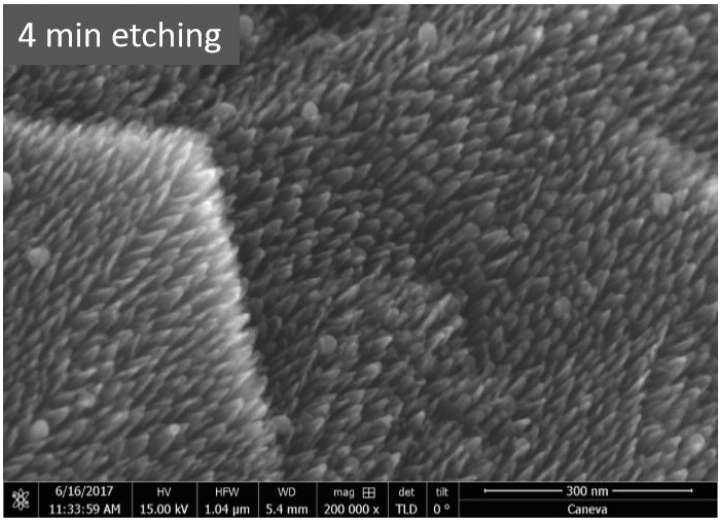

Figure 4.3: High resolution SEM figure under a tilted angle of 45 ° of BDD structured with diamond nanowires and gold particles on top of these wires. An etching time of 4 minutes was used.

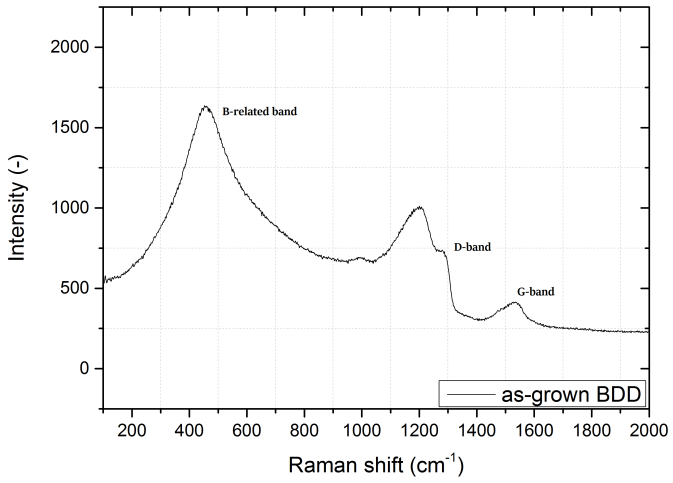

Figure 4.4: Raman spectrum of as-grown BDD

BDD electrode was used in two different ways: cleaned in acetone/ethanol/demi-water and after cleaning with strong acids. Preferably, the strong acid cleaning procedure contains three steps[53]. First, adsorbed organic matters are removed by ultrasonic cleaning in acetone, ethanol and deionized water, respectively. In between the different cleaning solutions (acetone, ethanol and demi-water), the electrode is rinsed with deionised water. In the second cleaning step, non-diamond and metal impurities are removed. This is done by a strong acid cleaning process. Nitric acid, sulfuric acid and chloridic acid are mixed together with a ratio of 1:1:1 and this solution is heated up to clean the electrodes. This cleaning step is finished when the colour of the strong acidic solution became transparent. Figure 4.6 shows cyclic voltammograms before and after strong acid cleaning[54].

As a final step, the electrodes are ultrasonically cleaned with deionized water for ten minutes to make sure that there are no acids left on the surface. Proper cleaning of the surface results in larger voltammetric responses and higher electron transfer rates[54].

A reset of the electrode is achieved by cycling in HNO_3. The potential window is measured and the surface becomes hydrophilic (oxygen-terminated).

By cleaning the as-grown BDD sample only with acetone/ethanol/demi-water, the as-grown hydrogen-terminated surface remains.

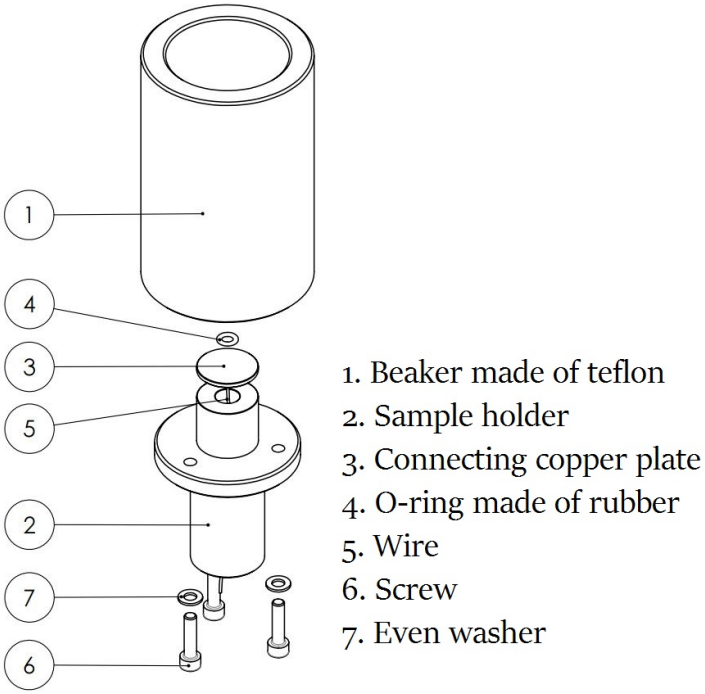

Figure 4.5: Constructed electrochemical cell apparatus

The RE and CE were cleaned by rinsing them a few times with demi-water and they were dried with air. The Teflon-beaker was cleaned with soap and water and afterwards rinsed with demi-water.

4.2.3. Electrochemical instruments

All electrochemical measurements, CV and EIS, were performed with the multi channel potentiostat from the company Metrohm Autolab b.v. The program Nova with version 1.10 was used to analyse the results of the EIS.

For CV measurements different parameters were varied. Measurements with different scan rates are performed with six different scan rates: 0.025, 0.05, 0.1, 0.2, 0.4, and 0.8 V/s. The step size used for all CV measurements is 0.01 V and the stop potential is chosen as the middle potential value in the range taken. All EIS measurements are performed with the same variables. The frequency is taken from 0.1 Hz to 10000 $0Hz$, the amplitude is 0.01 V, the integration time is 0.125 s and the number of points taken is 50. The only variable that has different values per measurement is the formal potential, this is changed in advance of each EIS measurement.

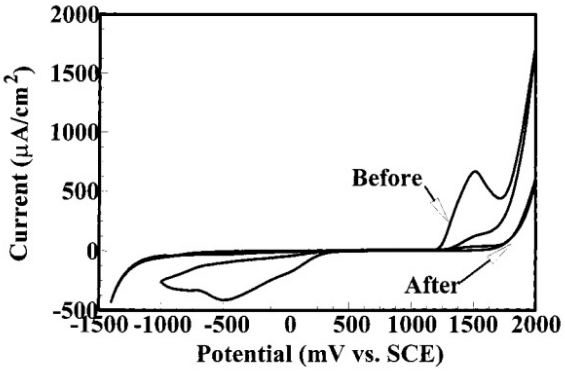

Figure 4.6: The effect of strong acid cleaning, reprinted from [54]

Before each measurement the solution is bubbled with nitrogen gas for at least one minute. The bubbling is done to remove oxygen dissolved in the solution. Then wait for thirty seconds to start the measurement, to be sure that the solution is stabilised.

All measurements were performed at 20 $^{\circ}C$, 293.15 K.

4.2.4. Chemicals used

All experiments were performed with demi-water from a water purification system (>15 $M\Omega cm$). All chemicals used (KCl, NaOH, ferrocyanide, ruhex, nitric acid, glucose) were all purchased from Sigma-Aldrich.

- Potassium chloride, ≥ 99%
- Sodium hydroxide pellets
- Potassium hexacyanoferrate(II)trihydrate, ≥ 99%
- Hexaaminеruthenium(III)chloride, 98%
- Nitric acid, 70%. Diluted to 5%
- D-(+)-Glucose, ACS reagent

All solutions were freshly prepared and thrown away on the day of use.

5

Results and discussion

The results of all measurements are discussed in this chapter. First, the results of measuring the potential window and background current of all electrodes in nitric acid are shown in Section 5.1. Then, the establishment of the standard characterisation protocol, followed by basic electrode characterisation with ferrocyanide and ruhex, is discussed in Section 5.2. Last, the results of the detection of glucose with all different (surface modified) electrodes, which are listed in Table 4.1, will be shown in Section 5.3.

5.1. Potential window and background current

The potential window and the background current of the diamond electrodes are determined in nitric acid (HNO_3). The scans were performed between -1 V and +2 V. The definition for the potential window maintained in this thesis is the potential range where the current densities are between plus and minus 200 $\mu A/cm^2$. The background current is the current measured in the absence of an analyte. This background current can be subtracted from the current response obtained with presence of an analyte. In this way a current density of zero will be seen in the background-corrected response when there is no analyte present in the solution[55].

Figure 5.1 shows the cyclic voltammograms of all different electrodes. It can be seen that the potential windows of samples 1a, 1b and 3 are similar (around 2.5 V). These are the as-grown, acid cleaned, and nanostructured BDD samples without gold present. Below potentials of -0.75 V and above 1.75 V the currents increase rapidly, this is due to water splitting. In between these potentials the curve is rather featureless, which is typical for diamond. There is a small difference in potential window visible for the as-grown and the acid-cleaned BDD. The acid-cleaned sample has a minimally wider potential window. This can has to do with the surface termination (oxygenated surface, in stead of hydrogenated) or because there are less impurities on the surface. By acid cleaning non-diamond and metal impurities are removed. The gold-containing electrodes show typical features for a gold electrode in an acidic solution. The anodic oxidation of gold nanoparticles starts from 1.05 V on the positive potential scan. The negative cathodic peaks around 0.9 V in the graphs of sample 2 and 4 are due to the reduction of gold oxides[56, 57]. The potential windows of these gold-particle-containing electrodes are a bit narrower, i.e. between 1.5 V and 2.25 V. The amount of gold on sample 2 is higher than on sample 4, which can be concluded from the magnitude of the redox peaks. This difference has to do with the etching process that took place at sample 4 to achieve the nanowires, as there is also some gold removed during this etching step.

The background currents can be read out in the zoomed figure, Figure 5.1b. The values are read out at 0.5 V and listed in Table 5.1. The higher background currents of samples 2, 3, and 4, has to do with the nanostructure, which is related to the surface roughness factor[30]. The gold-containing samples show even the highest background currents, this is due the fact that gold has a larger background current than diamond. Lower background currents are mainly due to a lower double layer capacitance, which is the case for the bare BDD samples. The potential windows and background currents are listed in Table 5.1.

It can be concluded that the potential windows of all samples are wide and the best for the BDD samples (as-grown, acid cleaned, and BDD+NWs), as expected for a diamond electrode. This is favourable for sensing applications.

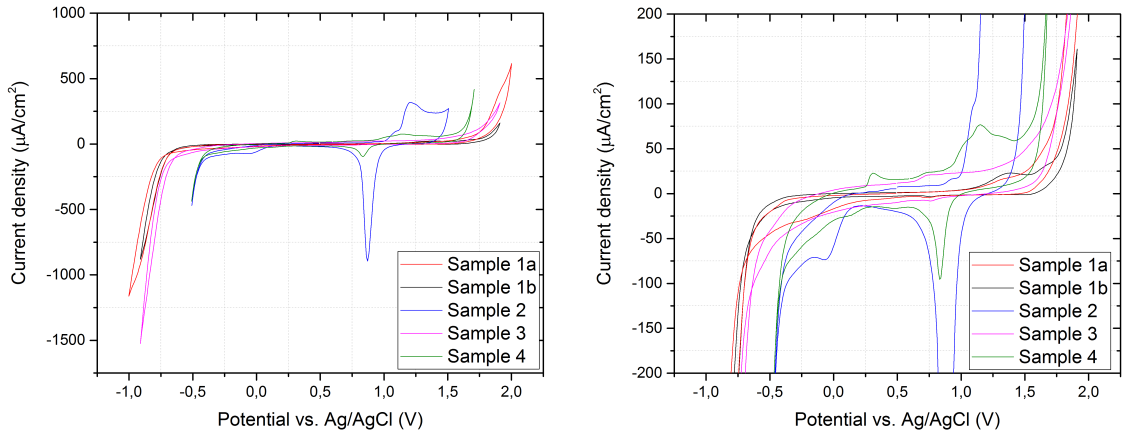

(a) (b)

Figure 5.1: CVs of the different diamond electrodes in 0.1 M HNO_3, 10th cycle is shown. Figure b) is a zoom of figure a)

Table 5.1: All used electrodes

Sample number	Sample description	Potential window in V	Background current in $\mu A/cm^2$
1a	as-grown BDD	2.65	5.08
1b	acid cleaned BDD	2.7	3.81
2	BDD with gold nano-islands	1.65	27.95
3	BDD with diamond nanowires	2.6	22.24
4	BDD with diamond nanowires and gold on top of the wires	2.15	31.77

5.2. Basic electrode characterisation

The results of the basic electrode characterisation are discussed in this section. The stabilisation of the electrode is described in Subsection 5.2.1. In Subsections 5.2.2 and 5.2.3 the results achieved in ferrocyanide and ruhex will be compared with results from literature. The kinetic parameters from the different electrodes were derived from EIS measurements in ferrocyanide and ruhex, are shown and discussed in Subsection 5.2.4.

5.2.1. Electrode stabilisation

At the beginning of doing measurements with bare BDD electrodes it was important to have an in depth look at the measurements to determine when a reliable measurement result is obtained. First, thirty cycles were measured to see how many cycles need to be performed to be sure that the signal is in equilibrium. The effects of doing measurements with and without nitrogen bubbling are observed as well. Figure 5.2a shows several cycles of a bare BDD electrode in 1 mM ferrocyanide and 0.1 M KCl at a scan rate of 0.1 V/s. The first cycle differs the most from the other cycles shown, the first cycles follows another path than the next cycles. Figure 5.2b shows the differences in current values for the oxidation peak. Again, it is visible that cycle 1 deviates the most of the other measured cycles. The peak current values from cycles 5 to 30 differ in the range of micro-amperes. The set-up reached equilibrium fast, after these results is chosen to measure at least 10 cycles for all experiments to be sure that the signal is reliable. A scan rate of 100 mV/s gives clear peak values and this scan rate is also often used in literature. The effects of nitrogen bubbling are also tested. Nitrogen is bubbled into the solution to expel and dissolve present oxygen. The effect of nitrogen bubbling was visible. There is chosen to bubble the solution for 1 minute before each measurement and then wait for thirty seconds to stabilise the solution.

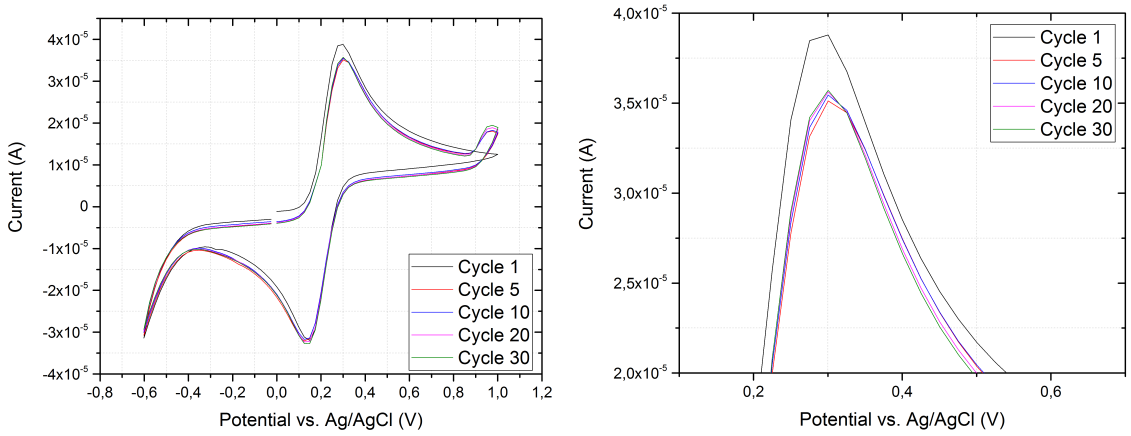

(a) (b)

Figure 5.2: CV of a flat diamond electrode in 1 mM ferrocyanide and 0.1 M KCl with a scan rate of 0.1 V/s, 30 cycles have been measured. Figure b) shows a zoom of Figure a)

5.2.2. Ferrocyanide

Ferrocyanide undergoes an inner-sphere electron transfer, as was explained in Section 2.4. The redox reaction that takes place is: $Fe(CN)_6^{4-} \rightleftharpoons Fe(CN)_6^{3-} + e^-$. Cyclic voltammetry were done with different scan rates and different molarities of ferrocyanide. The results are compared to data from literature.

Different scan rates in ferrocyanide

Measurements with different scan rates are performed to check the relationship between the peak current densities and the square root of the scan rates. This is one of the reversibility criteria, which were explained in Subsection 2.3.3. Figure 5.3b shows the CVs of sample 1a, sample 1b, and sample 3 in 1 mM ferrocyanide and 0.1 M KCl. The CVs of sample 1a and 1b look very similar, the biggest difference is the height of the peaks. Figure 5.3a shows a CV of the as-grown BDD electrode in 1 mM ferrocyanide and 0.1 M KCl at different scan rates. The increasing scan rates give higher peak values and shift the peaks more to the sides, which suggest a quasi-reversible or irreversible behaviour. Figure A.1 in Appendix A shows the CVs of all the electrodes in ferrocyanide, measured with different scan rates. The measurements with different scan rates are proceeded to see if the peak current is proportional to the square root of the scan rate, according to Randles-Sevcik equation. This was explained in Section 2.3.3 and has to do with the reversibility of the process. The linear relations are shown in Figure 5.4b. All three samples fit the linear fit pretty well. This proportionality between peak current densities and the square root of the scan rates mean state that the process is reversible. The peak-to-peak potential difference between samples 1a and 1b is similar (94 mV and 88 mV, respectively), while sample 3 has a larger peak-to-peak potential difference, 180 mV at a scan rate of 0.1 V/s. This larger peak-to-peak difference means that there is a smaller rate constant, and thus a slower electron transfer. The peak current density of sample 3 is in between the peak values of sample 1a and 1b, so the addition of diamond nanowires on the flat diamond electrode does not increase the peak current density significantly.

Comparison between experimental results and results from literature performed in ferrocyanide

The CVs of Figure 5.3 are compared to the literature results of diamond electrodes in ferrocyanide shown in Figure 5.5[54, 58]. The shapes of the CVs look similar and the values are in the same order of magnitude. The results from Figure 5.5b shows that the current peak values of the nanowires based electrode are a factor of 1.25 smaller than the values from the smooth diamond electrode. That behaviour can also be seen in Figure 5.3b. The smaller peaks measured for the nanostructured BDD electrodes have to do with the inner-sphere electrode transfer. This type of transfer is sensitive to the microstructure of the surface and the rate constant is highly dependent on the electrode's material. The addition of diamond NWs changes the microstructure of the electrode's surface and thereby decreases the rate constant.

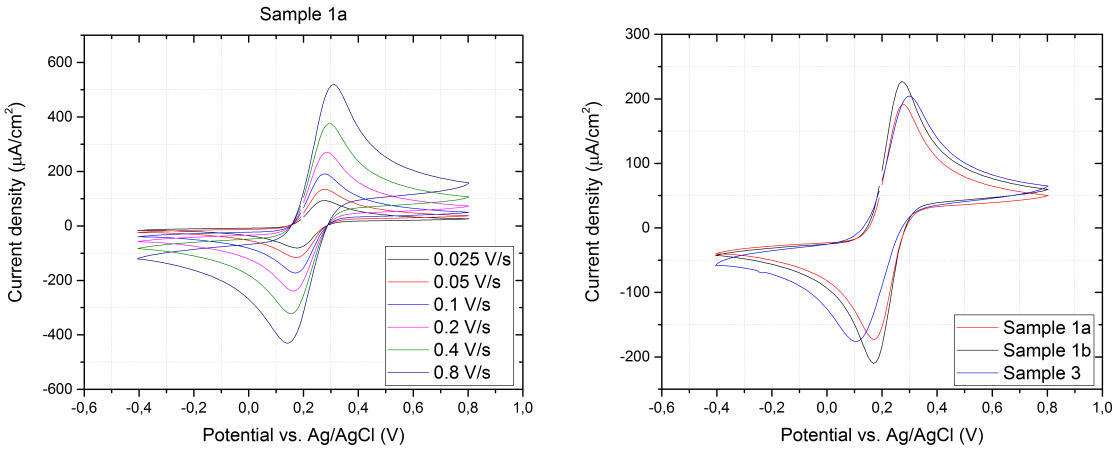

(a) (b)

Figure 5.3: a) CV of the as-grown BDD electrode in 1 mM ferrocyanide and 0.1 M KCl at different scan rates, 10th cycle is shown. b) CVs of different diamond electrodes in 1 mM ferrocyanide and 0.1 M KCl with a scan rate of 0.1 V/s, 10th cycle is shown.

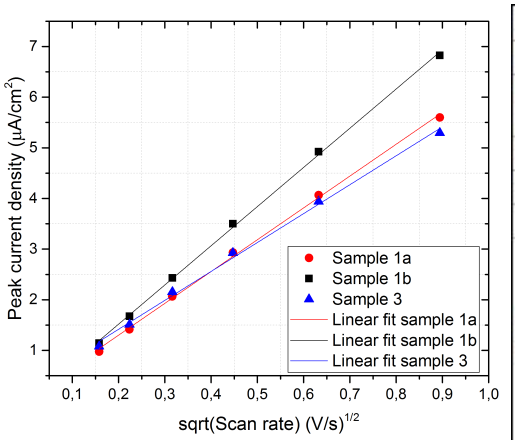

Equation	y = a + b*x		
Weight	No Weighting		
Residual Sum of Squares	0,01652	0,01928	0,03716
Pearson's r	0,99964	0,99937	0,99852
Adj. R-Square	0,9991	0,99842	0,99631
		Value	Standard Error
Peak current density	Intercept	-0,03014	0,05307
	Slope	7,73895	0,10358
	Intercept	0,04324	0,05733
	Slope	6,28434	0,11189
	Intercept	0,27483	0,07959
	Slope	5,71025	0,15534

(a) (b)

Figure 5.4: CVs in 1 mM ferrocyanide and 0.1 M KCl, 10th cycle is shown. Figure a) shows the linear relationship between the peak current densities and the square root of the scan rates. Figure b) shows the corresponding table to the linear fit.

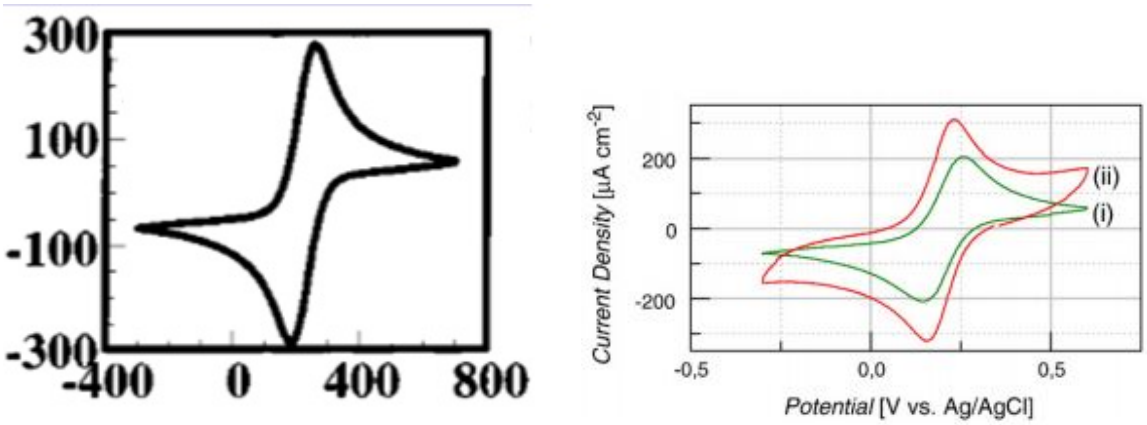

(a) (b)

Figure 5.5: CVs from literature of diamond electrodes in ferrocyanide. a) CV of a flat diamond electrode in 1 M KCl and 1 mM ferrocyanide, the y-axis shows the current density in $\mu A/cm^2$. Reprinted from [54]. b) CV of a diamond-NWs-based electrode (i) and smooth BDD (ii) in 0.1 M KCl and 1 mM ferrocyanide at a scan rate of 50 mV/s, reprinted from [58]

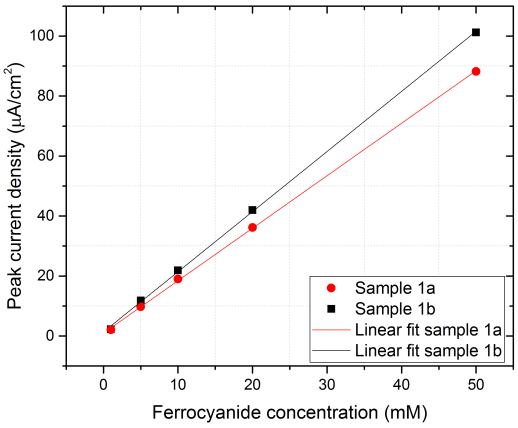

(a)

Equation	y = a + b*x		
Weight	No Weighting		
Residual Sum of Squares	2,18736	0,76596	
Pearson's r	0,99982	0,99992	
Adj. R-Square	0,99953	0,99978	
		Value	Standard Error
Peak current density	Intercept	1,35935	0,53411
	Slope	2,00458	0,02171
	Intercept	0,93088	0,31606
	Slope	1,75004	0,01285

(b)

Figure 5.6: a) linear relationship between the peak current densities and the different molarities of ferrocyanide for samples 1a and 1b. Figure b) shows the corresponding table to the linear fit.

Different molarities of ferrocyanide

Figure 5.6 shows the linear relationship between the peak current densities and the molarities of sample 1a and 1b in ferrocyanide. Sensitivities achieved are 1.75 $\mu A/mMcm^2$ and 2 $\mu A/mMcm^2$ for sample 1a and 1b, respectively. The sensitivity of the acid-cleaned BDD sample is higher than the sensitivity of the as-grown BDD. CVs of different samples with different molarities of ferrocyanide can be found in Figure A.3 More CVs on the remaining measurements can be found in Appendix A.

Last, measurements with sample 4 were performed in ferrocyanide. Sample 4 is the electrode made from BDD with diamond nanowires with gold nano-particles on top of it. By doing CV measurements with this sample in nitric acid before and after measuring in ferrocyanide, it was possible to see if there were changes in the electrode response. Figure 5.7 shows clearly a difference in response. The large peak that was first visible around 0.9 V almost completely disappeared after being used in ferrocyanide. This large peak is due to the gold particles, so the vanishing of the peak means that the gold is dissolved or transformed into another material. Probably, the cyanide ions form complex ions with the gold and this auricyanide, $(Au(CN)_4)^-$, is soluble[59].

From the results it can be concluded that the setup is working properly for the BDD electrodes. The graphs of cyclic voltammetry in ferrocyanide with BDD electrodes show similar results as the ones from literature,

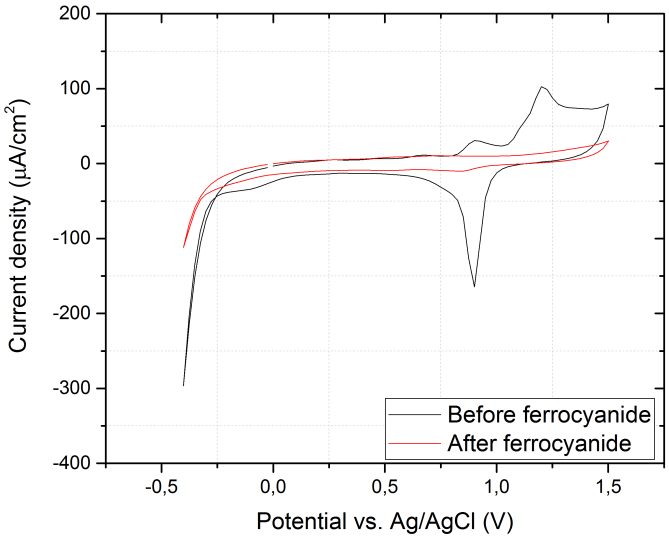

Figure 5.7: CV of sample 4 in 0.1 M HNO_3 before and after measuring in ferrocyanide

the shape and order of magnitude of the results is equal. Using ferrocyanide in combination with gold, as with sample 2 and 4, does not work out because the cyanide dissolves the gold.

5.2.3. Ruhex

Ruhex undergoes an outer-sphere electron transfer, which is already explained in Section 2.4. The reaction that takes place is: $Ru(NH_3)_6^{3+} \rightleftharpoons Ru(NH_3)_6^{2+} + e^-$. Cyclic voltammetry is done with different scan rates and different molarities of ruhex. The results are compared to data from literature.

Different scan rates in ruhex

In Figure 5.8a the reaction of different diamond electrodes in 1 mM ruhex and 0.1 M KCl is shown. The acid cleaned samples, sample 1b and 3, show the highest peak current densities, the sample with nanowires has even higher peaks than the flat BDD. The shapes of the CVs look very similar. The graphs show deviations from the expected path the graph normally follows at the potentials lower than -0.5 V, the normal path is shown in Figure 5.9b. It could be that there is a side reaction at this lower potentials, which causes the extra peaks at the lower potentials. The linear fitting of the peak current densities with the square root of the scan rate is shown in Figure 5.8b. For fitting is assumed that the peaks at the lower negative potentials are not there, otherwise it was not possible to draw a fitted baseline. All different samples show almost perfect linear behaviour. Ruhex is relatively insensitive to the surface termination and the microstructure of the surface, which is also visible in the linear relationship. As expected, the sensitivities of all samples are similar.

Comparison between experimental results and results from literature performed in ruhex

Figure 5.9 shows results from literature of diamond electrodes in ruhex[40, 54]. The graphs from literature, that can be seen in Figure 5.9, does not show these curvy lines. This can have to do with the smaller potential window that is used during measurements. The peak current densities measured have the same order of magnitude as the values from literature. Note that Figure 5.9b shows quite low current values, but the unit that is used here is μA instead of $\mu A/cm^2$ and the concentration of ruhex is 0.1 mM in stead of the 1 mM used in this research.

Different molarities of ruhex

Figure 5.10 shows the linear fit between the peak current densities and the molarities. The linear fit is almost perfect. The sensitivities obtained are 1.94, 2.20, and 1.97, for samples 1a, 1b, and 4, respectively.

Appendix B shows more graphs of the measurements performed in ruhex, like the CVs performed in different molarities of ruhex.

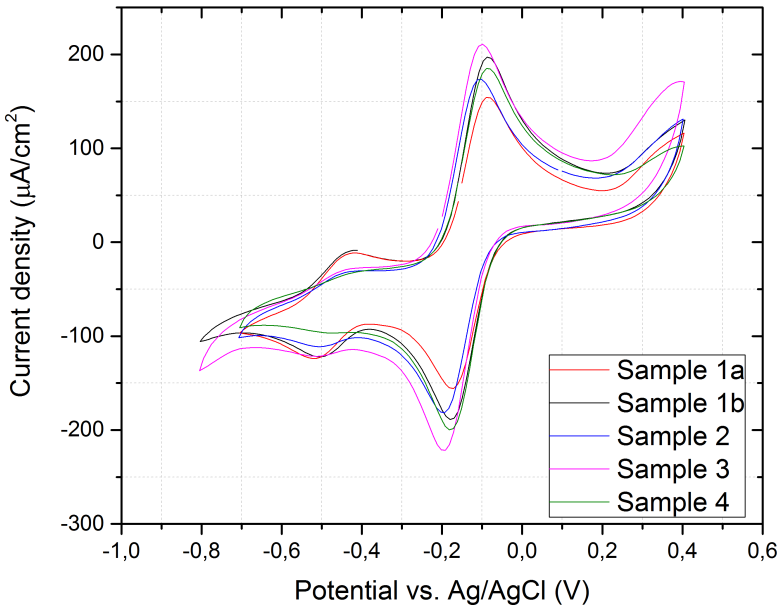

(a)

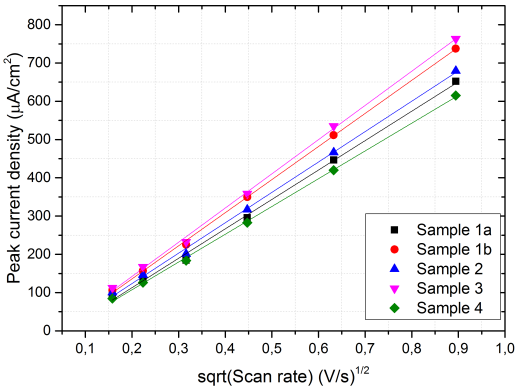

(b)

Equation	y = a + b*x				
Weight	No Weighting				
Residual Sum of Squares	576,0904	171,13182	375,40066	328,90315	162,91357
Pearson's r	0,99874	0,9997	0,99923	0,99947	0,9996
Adj. R-Square	0,99684	0,99926	0,99807	0,99867	0,999
		Value	Standard Error		
Peak current density	Intercept	-40,96862	9,90907		
	Slope	768,77892	19,34053		
	Intercept	-37,20108	5,40074		
	Slope	864,92056	10,54116		
	Intercept	-35,26567	7,99899		
	Slope	794,2584	15,61243		
	Intercept	-36,64989	7,48724		
	Slope	893,99674	14,61359		
	Intercept	-37,87618	5,26946		
	Slope	725,83256	10,28494		

(c)

Figure 5.8: CVs in 1 mM ruhex and 0.1 M KCl, 10th cycle is shown. Figure a) shows a CV of the different diamond electrodes with a scan rate of 0.1 V/s, Figure b) shows the linear relationship between the peak current densities and the square root of the scan rates and Figure c) shows the corresponding table to the linear fit.

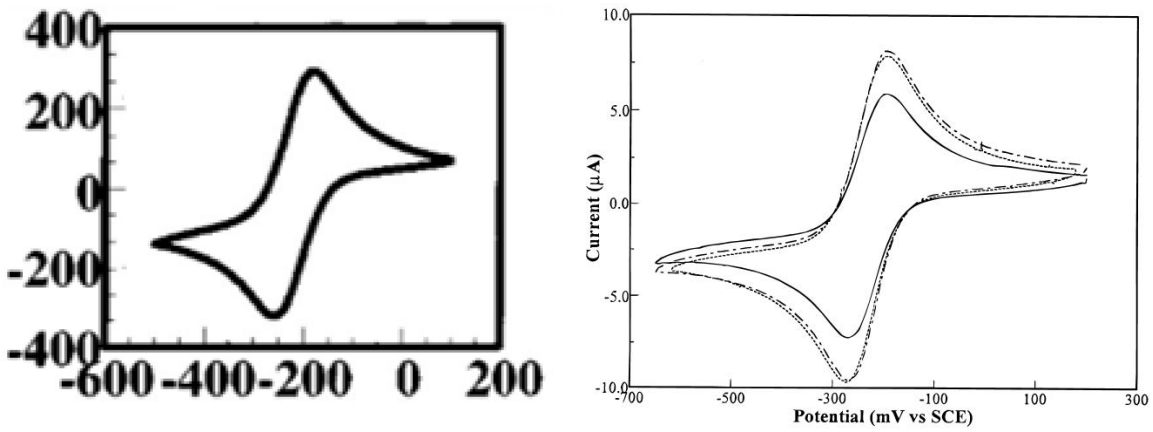

(a) (b)

Figure 5.9: CVs from literature of diamond electrodes in ruhex. a) CV of a flat diamond electrode in 1 M KCl and 1 mM ruhex, the y-axis shows the current density in $\mu A/cm^2$. Reprinted from [54]. b) CV of an as-grown (dotted line), an anodically polarised (solid line), and an acid washed and rehydrogenated (dash-dotted line) BDD electrode in 1 M KCl and 0.1 mM ruhex and exposed surface area of 0.2 cm^2. Reprinted from [40].

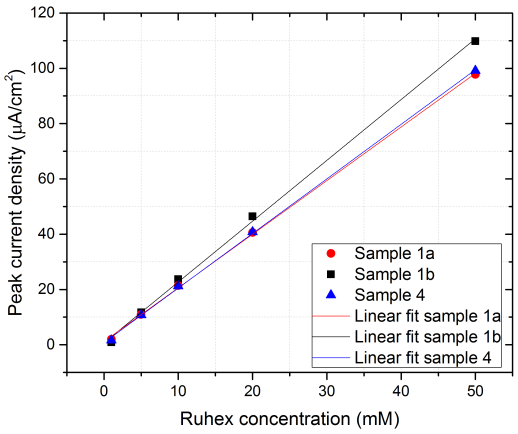

Equation	y = a + b*x		
Weight	No Weighting		
Residual Sum of Squares	8,9913	2,62878	2,06421
Pearson's r	0,9994	0,99977	0,99983
Adj. R-Square	0,9984	0,9994	0,99954
		Value	Standard Error
Peak current density	Intercept	0,70352	1,08289
	Slope	2,19976	0,04402
	Intercept	1,19322	0,58553
	Slope	1,93955	0,0238
	Intercept	0,76259	0,51886
	Slope	1,97451	0,02109

(a) (b)

Figure 5.10: Figure a) shows the linear relationship between the peak current densities and the different molarities of ruhex in 0.1 M KCl and a scan rate of 0.1 V/s, 10th cycle is shown. Figure b) shows the corresponding table to the linear fit.

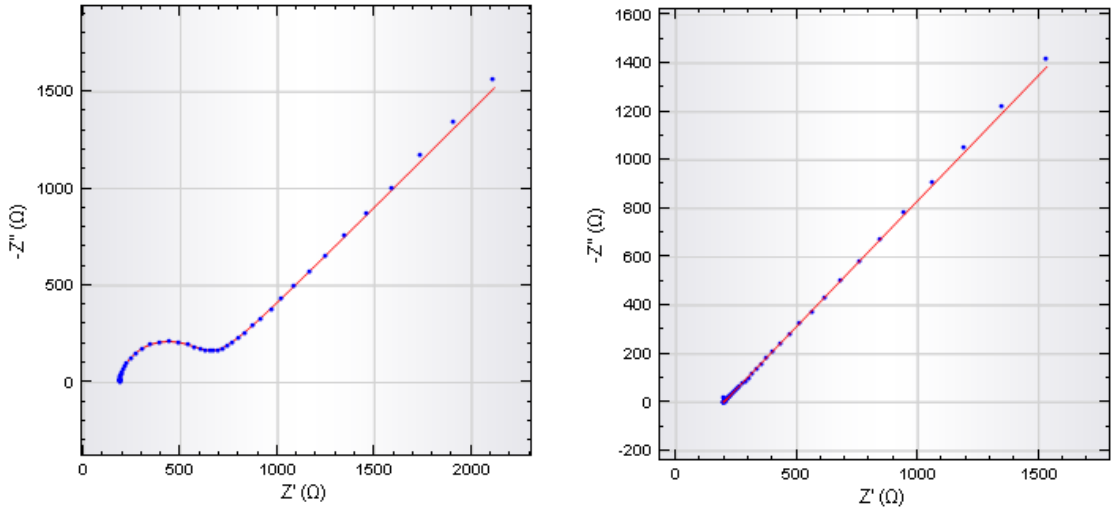

(a) (b)

Figure 5.11: Fitting of EIS data for sample 1a in a) 1 mM ferrocyanide, and b) 1 mM ruhex

5.2.4. Kinetics of ferrocyanide and ruhex

It is possible to compare the differences in kinetics between the different electrodes. The electron transfer rate constant k_0 is determined with Nicholson's method as well as with the fitting of the results from electrochemical impedance spectroscopy, both methods are explained in Section 2.3. Two fittings of sample 1a in ferrocyanide and ruhex are shown in Figure 5.11. The shapes of the Nyquist plots are similar for all electrodes. The shape of the Nyquist plot obtained in ferrocyanide show all a semi-circle followed by a straight line under an angle. The shape of the plot obtained in ruhex show all just a straight line under an angle, this makes it harder to achieve a good fitting. The results obtained are shown in Table 5.2. More detailed information about the EIS parameters can be found in Appendix C.

Table 5.2: Final results of different electrodes in 1 mM ferrocyanide and 1 mM ruhex at a temperature of 293 K and a scan rate of 100 mV/s, results are taken from the 10th cycle

		Nicholson's method		EIS	
Analyte	Sample	ΔE_p in mV	k_0 in $\mu m/s$	R_{CT} in Ω	k_0 in $\mu m/s$
$Fe(CN)_6^{3-/4-}$	1a	94	56.27	435.5	27.60
	1b	88.3	83.56	132.60	90.50
	3	180	18.23	1218	9.85
$Ru(NH_3)_6^{2+/3+}$	1a	78	117.51	80.96	148
	1b	81	133.03	77.32	155
	2	80	123.2	103	117
	3	81.6	138.7	18.65	644
	4	81.2	116.4	11.25	1070

The smaller the peak-to-peak potential, ΔE_p, the larger is the transfer rate constant. There is an exponential relation between ΔE_p and k_0, the graph reaches an equilibrium for higher ΔE_p-values. A higher peak-to-peak separation gives a lower transfer rate constant and this means that there is slower kinetics.

The transfer rate constants for ruhex achieved with Nicholson's method are very similar for all electrodes, while the values for ferrocyanide differ much more. The rate constants for ferrocyanide are at least one order of magnitude smaller than the rate constants for ruhex. This has to do with the different electron transfer mechanisms. Ferrocyanide has an inner-sphere electron transfer, this type of transfer is really sensitive to the surface termination and the microstructure of the surface. Samples 1b and 3 are both acid cleaned, but the transfer rate constants of these electrodes differ a lot. The difference between sample 1b and 3 is the surface structure, sample 1b has a flat surface whereas sample 3 has diamond nanowires on the surface. It can be

concluded that the oxygenated surface has less influence on the transfer rate constant than the structuring of the surface. Ruhex has an outer-sphere electron transfer and is insensitive to the surface terminations and the microstructure of the surface. With this knowledge it is logical that ferrocyanide has more diverse transfer rate constants for the different electrodes than ruhex has. The results obtained by EIS measurements show similar results for the ferrocyanide measurements. A larger peak-to-peak potential difference means a higher charge transfer resistance R_{CT} and a lower transfer rate constant for the measurements in ferrocyanide. The results obtained by Nicholson's method for the experimental results of the measurements performed in ruhex does not show the expected behaviour (higher peak-to-peak potential differences means lower transfer rate constants). Nicholson's method is only usable for quasi-reversible systems. The peak-to-peak potential differences of the measurements in ruhex are much more similar than these values for measurements in ferrocyanide. The measurements in ruhex show less reversible behaviour than the measurements in ferrocyanide; the peak-to-peak potential differences of measurements in ruhex at different scan rates differ less than the ones of measurements in ferrocyanide. Another requirement for making use of Nicholson's method is that the values for alpha need to be between 0.3 and 0.7 for valid results, which is not the case for the measurements done in ruhex. This means that the numbers obtained by Nicholson's method for the measurements done in ruhex are not to be trusted. Higher transfer rate constants, calculated by EIS, correspond to lower charge transfer resistances. Deviations can be due to the fitting of the Randles' circuit to the measured EIS data. To be sure that the fit is good enough, Pearson's chi-squared test is used. This test uses a measure to check the goodness of the fit. Chi-squared can be calculated by taking the sum of differences between the observed and expected outcome frequencies to the power of two and divide this by the expected outcome frequencies[60]. The smaller the chi-squared-value, the smaller the error. The χ^2-values of all fittings are listed in Table C.1 in Appendix C. It can be seen that the errors are all very small, ranging from 10^{-2}-10^{-4}. The kinetics for both ruhex and ferrocyanide is slightly better after acid cleaning for the bare BDD samples. This is because during acid cleaning sp^2-carbon and other impurities are removed.

Obvious is that the samples with nanowires, sample 3 and 4, obtain a one order of magnitude lower k_0 than the bare BDD sample in ferrocyanide and the same order and one higher order of magnitude for k_0 than the bare BDD in ruhex. This has to do with the type of electron transfer, inner-sphere and outer-sphere.

Another interesting thing to discuss is the reversibility of the measurements in ferrocyanide and ruhex on the different electrodes. The reversibility criteria are all explained in Section 2.3.3. From criteria 1 and 2 follows that all experimental results are quasi-reversible. From criteria 3 and 4 follows reversible behaviour and from criterion 5 that the process is not reversible. It can be concluded that all electrodes have a quasi-reversible behaviour in ferrocyanide, as well as in ruhex.

5.3. The detection of glucose

5.3.1. Measurements in glucose

Measurements in glucose are done for all five different electrodes. With some electrodes it was possible to detect the glucose, with others not. Figures 5.12 and 5.13 show CVs of the detection of glucose at all electrodes. Peaks can be clearly seen in the cyclic voltammograms of samples 1a, 2 and 4, although samples 1b and 3 show no peaks.

An important aspect in detecting glucose is the surface termination. As-grown BDD has a hydrogen terminated surface, while the acid cleaned BDD has an oxygen terminated surface. It appears to be the case that glucose can not be detected on an oxygen-terminated surface.

The gold-containing electrodes have a two-step anodic response to glucose during the positive scan. The glucose oxidation occurs on the forwards scan from about -0.6 V for sample 2 and from about -0.5 V for sample 4. The first anodic peak on the forward scan for sample 2 and sample 4 is around -0.5 V and -0.4 V, respectively[55, 56, 57]. After this small peak, the glucose oxidises further up to potential values between 0.2 V and 0.4 V. On the backward scan an intense re-oxidation peak of glucose is observed around 0.2 V[55, 57]. Increasing molarities shift all peaks a bit to the more positive potentials.

The gold that is on samples 2 and 4 increases the signal intensity one order of magnitude and works like an electrocatalyst. Making use of electrocatalysts is interesting for direct non-enzymatic glucose sensing because sensing glucose with bare BDD is a kinetically very slow process, often no visible peaks are observed[61]. The intensity of the peaks for the gold-decorated samples differ, the BDD+gold-sample has peaks twice as big as the BDD+NWs+gold-sample. From Figure 5.1 it was already clear that sample 2 contains more gold than sample 4; the gold peak around 0.9 V is larger for sample 2.

Figure 5.14 shows graphs of samples 2 and 4 cycling in nitric acid, measured before and after measuring

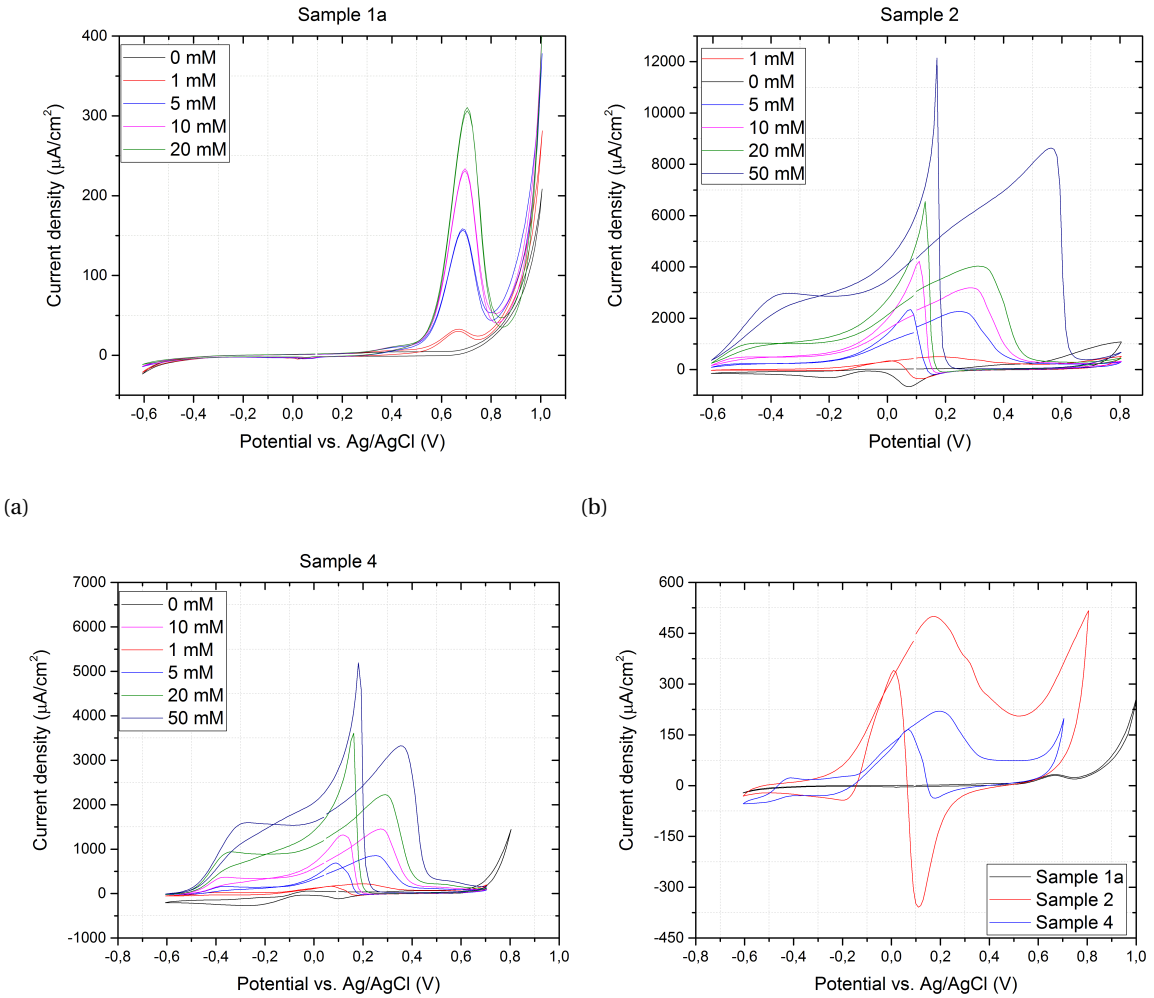

Figure 5.12: a), b) and c) show CVs of electrodes 1a, 2 and 4 in 0.1 M NaOH and different molarities of glucose and a scan rate of 0.1 V/s. d) shows a CV of these three electrodes with 1 mM of glucose and a scan rate of 0.1 V/s

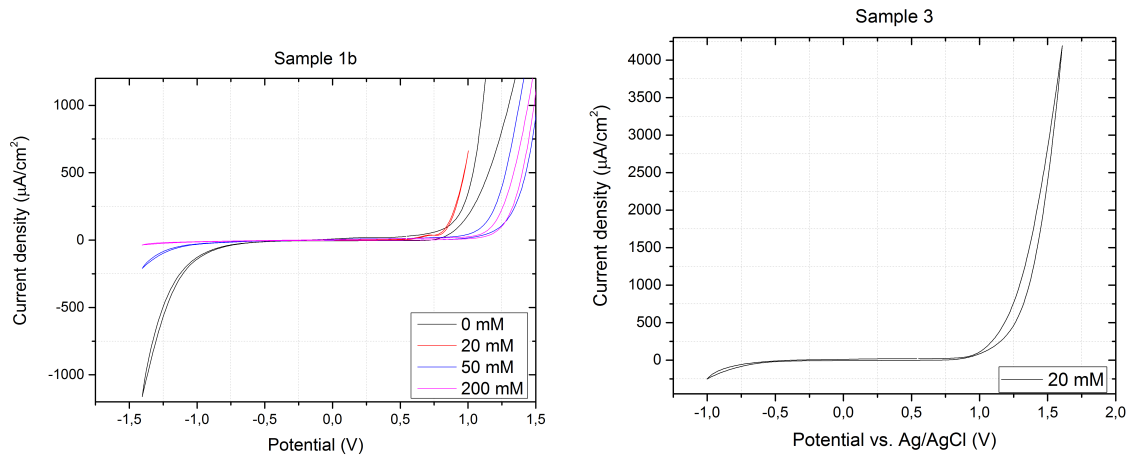

(a) (b)

Figure 5.13: a) CV of electrode 1b in 0.1 M NaOH and different molarities of glucose, and b) CV of electrode 3 in 0.1 M NaOH and 20 mM glucose

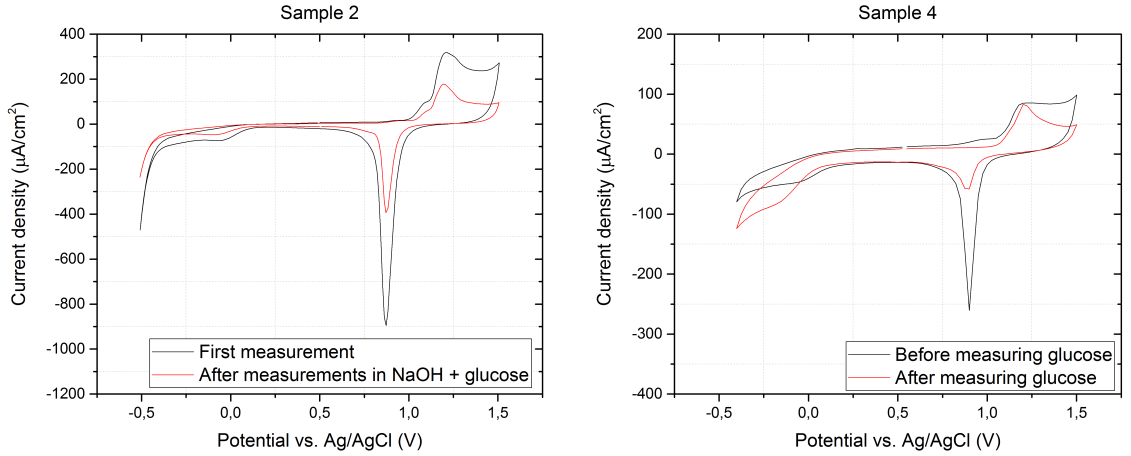

Figure 5.14: CVs of electrodes 2 and 4 in 0.1M HNO_3, measured before and after glucose sensing

glucose. It can be seen that the gold peak decreased, this means that the gold is dissolved during measuring glucose.

5.3.2. Mathematical relations between peak current densities, scan rates and molarities

All anodic and cathodic peaks are checked if there are mathematical relations between the peak current densities and the square root values of the scan rate and molarities. Before all fittings, the data are corrected for the background current. This background-corrected response is obtained by subtracting the values of the response obtained in the absence of glucose. The linear fitting of the peak current values with the square root of the scan rate does not fit well for sample 1a, as can be seen in Figure D.2a. When the data points of the two lowest scan rates, 0.025 V/s and 0.5 V/s, are dismissed, there is a good linear fit. Results from another as-grown BDD sample are observed as well, these CVs are shown in Figure FIGUUR. This linear fit is also very poor. This means that there is a non-diffusion controlled process for the as-grown BDD electrodes[61]. Figure D.3a shows good linear behaviour between the peak current densities and the square root of the scan rate for all peaks of sample 4, and for the higher scan rates of sample 1a. Sample 4 has a diffusion-controlled electron transfer for sensing glucose.

The linear fit between the peak current densities and the molarities of glucose is really poor, as can be seen in Figure D.3b. It looks like there is no linear relationship between the peak current densities and the

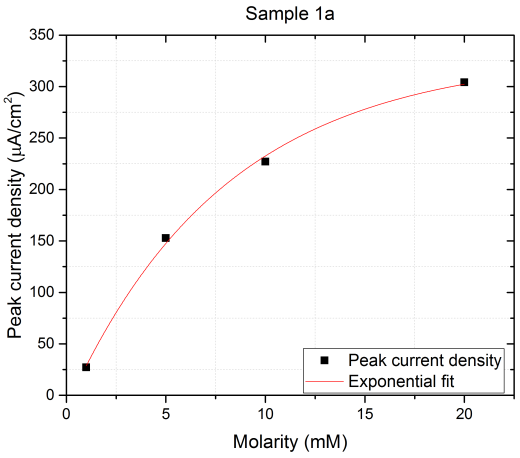

Model	Exponential		
Equation	y = y0 + A*exp(R0*x)		
Reduced Chi-Sqr	62,91591		
Adj. R-Square	0,99548		
		Value	Standard Error
Peak current density	y0	330,29168	15,84475
	A	-341,81851	14,88677
	R0	-0,12521	0,01621

Figure 5.15: Exponential fitting of peak current densities and molarities of sample 1a

Table 5.3: Results of the performance of the BDD samples for detecting glucose

Sample	Sensitivity in $mA/mMcm^2$	Linear range in mM
1a	0.022	1-10
2, left peak	0.429	1-10
2, right peak	0.294	1-10
4, left peak	0.129	1-10
4, right peak	0.136	1-10

molarities. However, the relations look more exponential. After fitting, almost perfect exponential fittings are achieved for sample 1a, the left peak of sample 2 and the right peak of sample 4, which can be seen in Figures 5.15, 5.16, and 5.17. The exponential fittings for the right peak of sample 2 and the left peak of sample 4 have still a maximum error of 5 percent, so they can be assumed exponential as well. A possible reason for this exponential relationship is that the boron sites on the electrode's surface of the electrode is saturated at some point, it is expected that the graph reaches an equilibrium at higher glucose molarities[44].

In Appendix D, all measurements performed in glucose can be found.

5.3.3. Sensitivities and linear ranges

Important for the performance of the glucose sensors are the sensitivity and the linear detection range. The sensitivity is the slope of the graph with linear fit between the peak current densities and molarities in $\mu A/mMcm^2$. First, a linear fit was performed with all data points, as is shown in Figure D.3b. Unfortunately this fit was rather poor, so new fitting was done for smaller molarity ranges, which is shown in Figure 5.18. The samples show much better linear fit for molarities between 1 mM and 10 mM. The sensitivities and linear ranges are shown in Table 5.3.

The highest sensitivities are achieved with sample 2, the BDD+gold electrode, followed up by the sensitivities of sample 4. The poorest sensitivities are achieved with the as-grown BDD electrode. The linear range is for all samples 1 mM to 10 mM. The molarity range from 1-10 mM is the most important range for the detection of glucose in human blood. The linear ranges could have been more precise and diverse when more data points were measured in the lower molarities range.

5.3.4. Comparison between experimental results and results from literature

Figure 5.19 shows results from literature for electrodes that contain gold. Compared to Figures 5.12b and 5.12c it can be seen that these graphs have similar-shaped CVs with the anodic and cathodic peaks at similar potentials. The peak current densities of the measurements are higher than the ones from literature. This has probably to do with the higher scan rates used during this thesis, the amount of gold on the exposed surface area of the electrode and the materials being of different grade.

Mathematical fittings are done between peak current densities and molarities of glucose. These results,

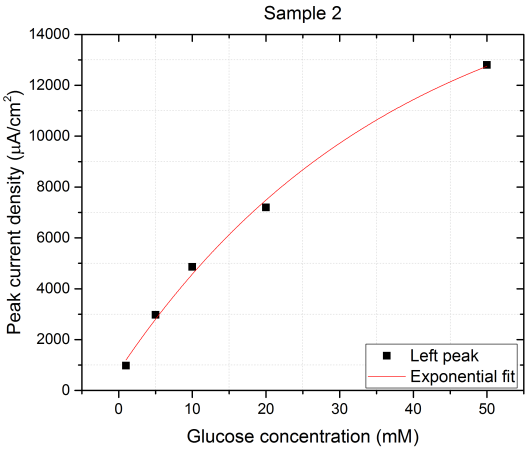

Model	Exponential		
Equation	y = y0 + A*exp(R0*x)		
Reduced Chi-Sqr	125741,39194		
Adj. R-Square	0,99394		
		Value	Standard Error
Peak current density	y0	17080,07268	1938,09281
	A	-16306,49822	1766,54382
	R0	-0,02652	0,00593

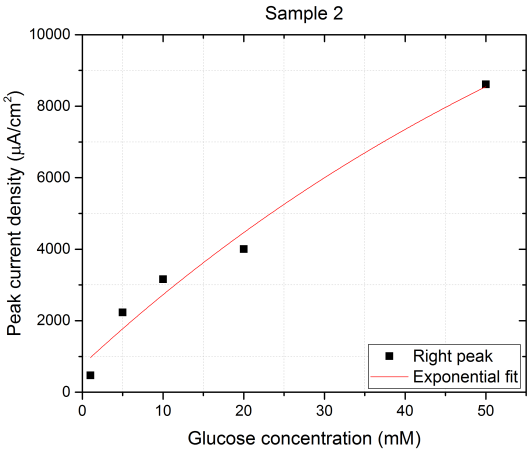

Model	Exponential		
Equation	y = y0 + A*exp(R0*x)		
Reduced Chi-Sqr	430378,15694		
Adj. R-Square	0,95355		
		Value	Standard Error
Peak current density	y0	17530,88712	16328,60073
	A	-16772,84455	15937,98286
	R0	-0,01248	0,01675

Figure 5.16: Exponential fitting of peak current densities and molarities of sample 2

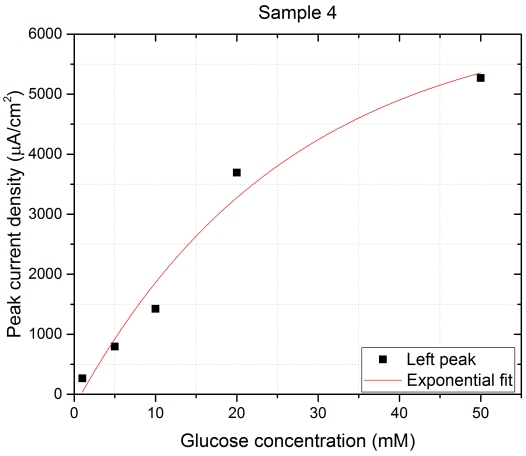

Model	Exponential		
Equation	y = y0 + A*exp(R0*x)		
Reduced Chi-Sqr	220192,39178		
Adj. R-Square	0,95088		
		Value	Standard Error
Peak current density	y0	6333,69889	1331,07343
	A	-6541,3871	1178,59073
	R0	-0,03798	0,01762

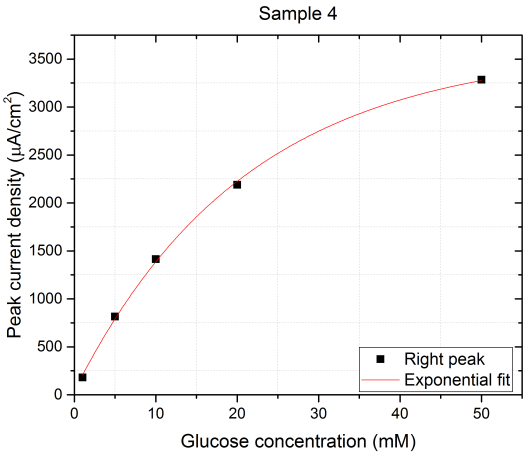

Model	Exponential		
Equation	y = y0 + A*exp(R0*x)		
Reduced Chi-Sqr	1630,37767		
Adj. R-Square	0,99888		
		Value	Standard Error
Peak current density	y0	3612,34961	81,41628
	A	-3571,98162	74,48637
	R0	-0,04729	0,00275

Figure 5.17: Exponential fitting of peak current densities and molarities of sample 4

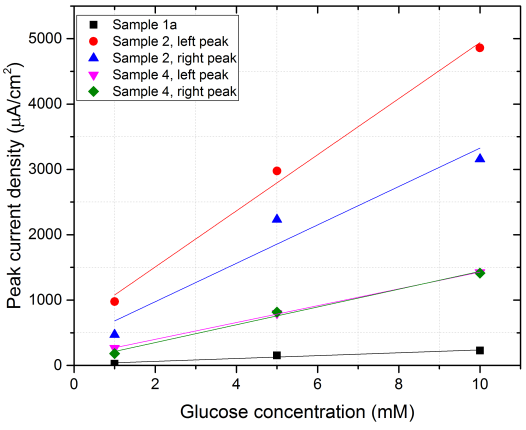

Equation	y = a + b*x				
Weight	No Weighting				
Residual Sum of Squares	897,94874	48766,29142	214613,02693	178,79932	4967,0087
Pearson's r	0,97779	0,99676	0,97077	0,99987	0,99672
Adj. R-Square	0,91215	0,98707	0,8848	0,99947	0,98691
		Value	Standard Error		
Peak current density	Intercept	18,75554	30,45307		
	Slope	21,92234	4,69901		
	Intercept	648,18991	224,42189		
	Slope	429,26001	34,62905		
	Intercept	387,37454	470,79669		
	Slope	293,84477	72,64551		
	Intercept	142,09866	13,58902		
	Slope	128,68038	2,09683		
	Intercept	77,73785	71,62305		
	Slope	136,14659	11,05168		

(a) (b)

Figure 5.18: Linear fit between peak current densities and molarities

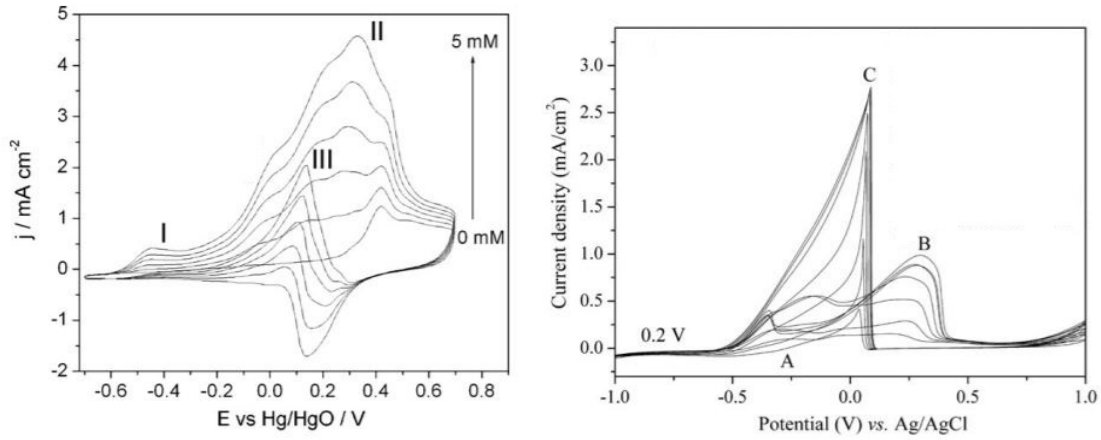

(a) (b)

Figure 5.19: a) CV curves of the AU NW array electrode in 0.1 M NaOH and glucose at concentrations of 1-5 mM, the scan rate is 50 mV/s. Reprinted from [56]. b) CV of glucose oxidation on a Au/DLC:P electrode at 50 mV/s in a 0.1 M NaOH solution with continuous glucose injection. Reprinted from [57]

Figure 5.18, are compared to results from literature, Figure 5.20[56, 57]. It was already mentioned in this Section that exponential fittings had a better fit than the linear fittings, especially for the wider molarity ranges. Having a look at the linear fittings of literature shows that the measured peak current values at higher molarities deflect as well. Probably there is also an exponential fitting that fits these results better than these linear fits.

The sensitivities and linear detection ranges from these literature reports are listed in Table 5.4 together with the experimental results from this thesis Sensitivities of all the left peaks (left peak, peak III and peak C) are in the same order of magnitude. The highest sensitivities are achieved with the gold nanowire array electrode, then sample 2, then sample 4 and last the phosphorous-doped diamond-like carbon with gold nanostructures. The same ranking is achieved from high to low sensitivities for the right peaks (right peak, peak II and peak B). The sensitivity of the phosphorous-doped diamond-like carbon with gold nanostructures is one order of magnitude smaller than the others. So, good representative sensitivities can be achieved with nanostructured and functionalised BDD, samples 2 and 4, for the detection of glucose.

Comparison can also be made between results from sample 1a, Figure 5.12a, and bare BDD electrodes in literature, Figure 5.21. Peak current densities for 5 mM glucose are 155 $\mu A/cm^2$, 500 $\mu A/cm^2$ and 480 $\mu A/cm^2$ for sample 1a, sample from source [44], and sample from source [45], respectively. These peak current densities are in the same order of magnitude. The sensitivities obtained for sample 1a and the sample from the paper of Zhao, et al. differ one order of magnitude, these sensitivities are also listed in Table 5.4. Surface termination is very important for the detection of glucose on bare BDD, as was already concluded before because it was possible to detect glucose with as-grown BDD and not with the acid-cleaned BDD. The sample used in the paper of Lee, et al. has had a hydrogen treatment before measurements. Differences in the peak current densities and sensitivities can have to do with the boron-doping levels of the electrodes.

All achieved results from measurements done for this thesis can also be compared to other literature results of sensing glucose with (modified) BDD that are listed in Table 2.3. The linear range from 1-10 mM is similar to results from the table. The largest difference is the smaller amounts that can be detected. It could be that this is also possible with the samples used in this thesis study, but this is not measured yet. Results of such high sensitivities for BDD with gold nanoparticles are not published yet, so this is a nice achievement that has a lot of opportunities for future research.

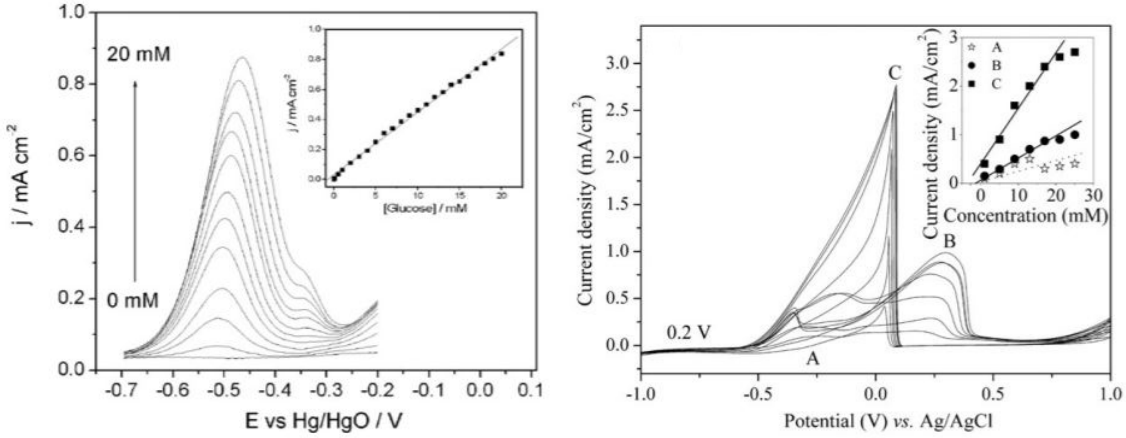

(a) (b)

Figure 5.20: CV curves and the linear fit of peak current densities and molarities: a) CV curves of the AU NW array electrode in 0.1 M NaOH and glucose at concentrations of 0.5-20 mM, the scan rate is 20 mV/s. The inset shows the linear fit. Reprinted from [56]. b) CV of glucose oxidation on a Au/DLC:P electrode at 50 mV/s in a 0.1 M NaOH solution with continuous glucose injection. Reprinted from [57]

Table 5.4: Results of the performance of the BDD samples for detecting glucose. *phosphorous-doped diamond-like carbon

Sample	Sensitivity in $mA/mMcm^2$	Linear range in mM	Source
1a	0.022	1-10	This thesis
2, left peak	0.429	1-10	This thesis
2, right peak	0.294	1-10	This thesis
4, left peak	0.129	1-10	This thesis
4, right peak	0.136	1-10	This thesis
Gold nanowire array electrode, peak II	0.960	0.5-14	[56]
Gold nanowire array electrode, peak III	0.728	0.5-14	[56]
DLC:P* with gold nanostructures, peak B	0.050	0.5-17	[57]
DLC:P* with gold nanostructures, peak C	0.095	0.5-17	[57]
Nanocrystalline BDD	101.9	0.25–10	[44]
BDD	-	0.5-10	[45]

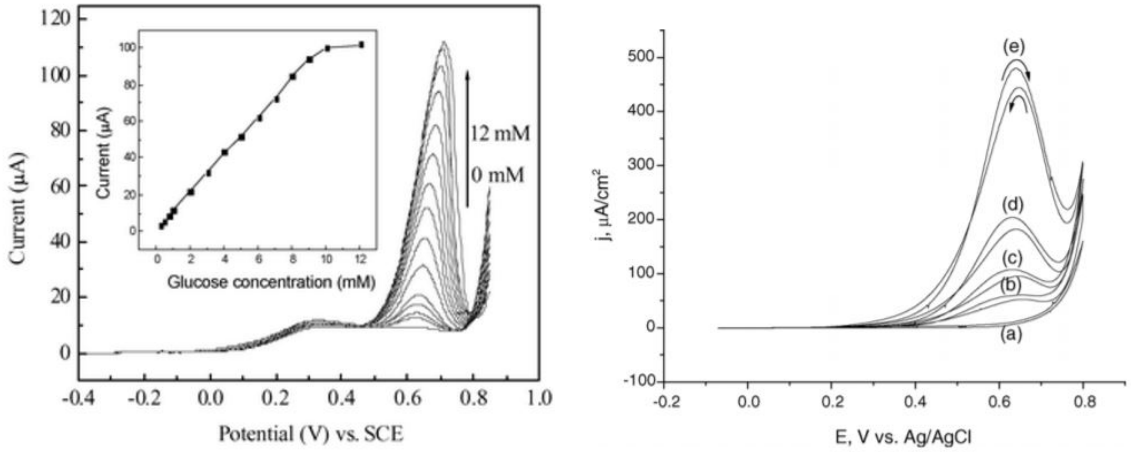

(a) (b)

Figure 5.21: a) Linear sweep voltammetry for different glucose concentrations in 0.1 M NaOH at a NCD BDD thin-film electrode in the presence of 0.5 mM AA and UA. The inset shows the relationship between glucose concentrations and peak currents in the range of 0.25-12 mM. The electrode area is 0.1 cm^2. Reprinted from [44]. b) CV different molarities of glucose (0, 0.5, 1, 2, and 5 mM) in 1 M NaOH at hydrogen-terminated BDD. The scan rate used is 20 mV/s. Reprinted from [45]

6

Conclusion

With the work done in this thesis, it can be concluded that direct non-enzymatic glucose sensing with unmodified, as-grown, BDD is possible. Redox peaks are clearly visible in the cyclic voltammograms after addition of glucose to the electrolyte solution. From the relation between peak current densities and the square root of the scan rates can be concluded that the electron transfer process is not a simple diffusion-controlled mechanism; the relation between these two parameters is not linear. However, glucose detection peaks are not visible for acid cleaned BDD samples. The same is true for BDD that is treated by oxygen plasma during reactive ion etching (RIE) to form diamond nanowires at the surface. By acid cleaning and the used RIE process, the surface termination changed from a hydrogen terminated to an oxygen terminated surface. So, the surface termination of the diamond electrode material is an important aspect in glucose sensing. The surface needs to be hydrogenated, instead of oxygenated, in order to be able to directly detect glucose.

The expectation was that increasing the exposed surface area by the addition of surface nanostructures increases the glucose signal as well. However, this did not emerge from the experimental results. Electrochemical measurements in ferrocyanide showed that the kinetics became worse on the BDD sample with nanowires with respect to the as-grown and acid-cleaned BDD samples; the electron transfer rate constant k_0 decreased and a one order of magnitude higher active charge transfer resistance R_{CT} was measured during electrochemical impedance spectroscopy. This effect is most likely on account of the electron transfer mechanism, which is an inner-sphere electron transfer process for ferrocyanide.

The functionalisation of a BDD surface was expected to increase the performance of the detection of glucose. The detection of glucose was indeed improved by the functionalisation of the surface with gold nanoparticles. The gold nanoparticles work like an electrocatalyst and much higher peak current densities were measured. The sample with BDD+gold+NWs showed good linear behaviour between the peak current densities and the square root of the scan rate for all peaks in the cyclic voltammogram. A drawback of the gold decorated samples is the instability. A decline in peak current densities is found in doing measurements in nitric acid with the gold-decorated samples before and after measuring with these samples in the glucose-containing electrolyte. This means that the modified BDD surface is not perfectly stable. Gold is dissolved or oxidised during the measurements, which causes the glucose detection peaks to decrease in magnitude.

Good linear behaviour is found for the as-grown BDD, BDD+gold, and BDD+gold+NWs electrodes for detecting glucose in the range of 1-10 mM. This is a suitable range for detecting glucose in human blood. The BDD+gold sample and BDD+gold+NWs sample have both two anodic peaks that show a good linear relationship between peak current densities and molarities. The right peak around 250 mV vs. Ag/AgCl is measured on the forward scan and belongs to the oxidation of glucose. The left peak around 80 mV vs. Ag/AgCl is measured on the backward scan, a re-oxidation of glucose took place. Both peaks can be used for the determination of the amount of glucose in the solution. Sensitivities achieved for as-grown BDD, left peak of BDD+gold, right peak of BDD+gold, left peak of BDD+gold+NWs, and right peak of BDD+gold+NWs are 0.022, 0.429, 0.294, 0.129, and 0.136 $mA/mMcm^2$, respectively. The sensitivity measured for as-grown BDD is one order of magnitude smaller then values reported in literature studies on bare BDD electrodes. The functionalised and structured electrodes, BDD+gold and BDD+gold+NWs, have sensitivities that are well in line with the sensitivities reported in literature studies for glucose sensing on structured, and functionalised, BDD electrodes. The only higher sensitivity reported in literature studies is achieved on a BDD electrode that is surface-modified with nickel nanoparticles.

The highest sensitivities are achieved with the BDD electrode functionalised with gold nanoparticles, followed up by the BDD electrode with gold nanoparticles and diamond nanowires, and the poorest sensitivity was on the bare BDD electrode. Making use of electrocatalysts is an interesting and useful functionalisation for direct non-enzymatic glucose sensing, because sensing glucose with bare BDD is a kinetically very slow process. Results of such high sensitivities for BDD with gold nanoparticles are not published yet, so this is a promising achievement that asks for continuation of research in this field.

The research done in for thesis will be useful for future work in catalytic detection of biomolecules and contaminants in water, in bodily fluids, and so on, in the form of more developed sensors (BioMEMS, microfluidic chips, etc.) made out of diamond.

7

Recommendations for future research

A first start on electrochemical sensing with boron-doped diamond (BDD) electrodes has been made in the diamond-group of department PME. It was found that sensing glucose with bare BDD is possible, but that the functionalisation of BDD with gold nanoparticles improved the sensing of glucose quite substantially. However, there are still several important unanswered questions and technological challenges that need to be addressed first. Among other, these are related to the understanding of the electrochemistry of BDD electrodes in the detection of glucose and the long-term stability of gold-decorated BDD electrodes. For this reason, some recommendations for further research are listed below.

- Electrochemical measurements with more data points in between the relevant concentration range need to be performed and repeated several times to see if BDD electrodes are suitable for measuring glucose in bodily fluids. Typical glucose concentrations in human blood, urine, and sweat are between 1-10 mM, 0-1 mM, and 0.01-1 mM, respectively. The sensitivity needs to be checked for lower concentrations of glucose.

- Examine if it is possible to detect molarities in the range 0.01-1mM, which is needed for detection in urine and sweat. It needs to be checked if there are, unwanted, interactions during the electrochemical measurements between the glucose oxidation/reduction peaks and the oxidation/reduction peaks of other substances in the fluid. The glucose detection peaks should still be visible and usable for determination of the amount of glucose in the fluid. Possible interfering species can be uric acid (UA) and ascorbic acid (AA), for instance.

- What is the effect of different electrode surface terminations on measuring glucose? In this thesis work it was concluded that it was only possible to detect glucose with a hydrogen-terminated BDD electrode, and not with the oxygen-terminated BDD electrode. Of course, also other terminations are possible and need to be researched. An interesting termination can be the addition of nickel particles. Very high sensitivities are already obtained with these particles in literature, maybe it is possible to optimise the detection of Ni-BDD electrodes in new research[47].

- Is it possible to have full control over the surface terminations of BDD? What surface termination works best for the detection of glucose? Is it possible to terminate the surface in a desired way? Are there easy ways to hydrogenate the BDD surface in a controlled manner?

- There is a recent paper about the nonenzymatic detection of glucose with a BDD functionalised electrode, bimetallic nanocatalysts are added to the surface for a better detection of glucose[51]. Platinum and gold nanoparticles are synthesised by electrodeposition on the surface of a BDD electrode. They were able to have greater activity and selectivity in detecting glucose. It can be interesting to research different combinations of metal nanoparticles to see which combinations have the best performance for the detection of glucose. Important performance indicators could be the sensitivity, the limit of detection and the linear range.

- Another interesting recent paper is published about the non-enzymatic sensing of glucose with a sensor based on CuO modified vertically-grown ZnO nanorods[62]. They used CuO (copper oxide) on ZnO

(zinc oxide) to have enhanced catalytic detection of glucose. CuO has not been used yet on BDD electrodes for the detection of glucose. A BDD electrode with CuO-modified BDD nanowires could be an interesting and novel functionalisation of diamond for the detection of glucose.

Bibliography

[1] Paul W May. Cvd diamond: a new technology for the future? *Endeavour*, 19(3):101–106, 1995.

[2] Huimin Liu and David S Dandy. *Diamond chemical vapor deposition: nucleation and early growth stages*. Elsevier, 1996.

[3] Paul W May. Diamond thin films: a 21st-century material. *Philosophical Transactions of the Royal Society of London A: Mathematical, Physical and Engineering Sciences*, 358(1766):473–495, 2000.

[4] Karl E Spear and John P Dismukes. *Synthetic diamond: emerging CVD science and technology*, volume 25. John Wiley & Sons, 1994.

[5] Julian Norley. technical brief: the role of natural graphite in electronics cooling. *Electronics Cooling*, 7:50–51, 2001.

[6] Matthew A Hopcroft, William D Nix, and Thomas W Kenny. What is the young's modulus of silicon? *Journal of microelectromechanical systems*, 19(2):229–238, 2010.

[7] LJ Vandeperre, F Giuliani, SJ Lloyd, and WJ Clegg. The hardness of silicon and germanium. *Acta Materialia*, 55(18):6307–6315, 2007.

[8] Stephen John Sque. *A first-principles study on bulk and transfer doping of diamond*. University of Exeter, 2005.

[9] Hugh O Pierson. Handbook of carbon, graphite, diamond, and fullerenes, processing, properties and applications, 1993.

[10] Jukka Rantala. technical data: diamonds are a thermal designer's best friends. *Electronics Cooling*, 8:10–11, 2002.

[11] EI Erlich and WD Hausel. W. diamond deposits, society for mining, metallurgy, and exploration. *Inc.(SME), Littleton, CO, USA*, 80127:374, 2002.

[12] Erik G Lundblad. High pressure synthesis of diamond in sweden in 1953. In *AIP Conference Proceedings*, volume 309, pages 503–506. AIP, 1994.

[13] Michael Schwander and Knut Partes. A review of diamond synthesis by cvd processes. *Diamond and related materials*, 20(9):1287–1301, 2011.

[14] Dr. Christoph Wild. Cvd diamond - faq, 2008.

[15] Yuan Yu, Liangzhuan Wu, and Jinfang Zhi. Diamond nanowires: Fabrication, structure, properties and applications. In *Novel Aspects of Diamond*, pages 123–164. Springer, 2015.

[16] EMA Fuentes-Fernandez, JJ Alcantar-Peña, G Lee, A Boulom, H Phan, B Smith, T Nguyen, S Sahoo, F Ruiz-Zepeda, MJ Arellano-Jimenez, et al. Synthesis and characterization of microcrystalline diamond to ultrananocrystalline diamond films via hot filament chemical vapor deposition for scaling to large area applications. *Thin Solid Films*, 603:62–68, 2016.

[17] DC Barbosa, PRP Barreto, VW Ribas, VJ Trava-Airoldi, and EJ Corat. Diamond nanostructures growth. *Encyclopedia of Nanoscience and Nanotechnology*, 10:3–10, 2009.

[18] Veronique Vermeeren, Sylvia Wenmackers, Patrick Wagner, and Luc Michiels. Dna sensors with diamond as a promising alternative transducer material. *Sensors*, 9(7):5600–5636, 2009.

[19] Yasuaki Einaga, John S Foord, and Greg M Swain. Diamond electrodes: Diversity and maturity. *Mrs Bulletin*, 39(6):525–532, 2014.

[20] YS Zou, Y Yang, WJ Zhang, YM Chong, B He, I Bello, and ST Lee. Fabrication of diamond nanopillars and their arrays. *Applied Physics Letters*, 92(5):053105, 2008.

[21] Nianjun Yang, Hiroshi Uetsuka, and Christoph E Nebel. Biofunctionalization of vertically aligned diamond nanowires. *Advanced Functional Materials*, 19(6):887–893, 2009.

[22] Hideki Masuda, Takashi Yanagishita, Kenji Yasui, Kazuyuki Nishio, Ichizo Yagi, Tata N Rao, Akira Fujishima, et al. Synthesis of well-aligned diamond nanocylinders. *Advanced Materials*, 13(4):247–249, 2001.

[23] Sabine Szunerits, Yannick Coffinier, and Rabah Boukherroub. Diamond nanowires: A novel platform for electrochemistry and matrix-free mass spectrometry. *Sensors*, 15(6):12573–12593, 2015.

[24] Yuan Yu, Liangzhuan Wu, and Jinfang Zhi. Diamond nanowires: fabrication, structure, properties, and applications. *Angewandte Chemie International Edition*, 53(52):14326–14351, 2014.

[25] Yannick Coffinier, Elisabeth Galopin, Sabine Szunerits, and Rabah Boukherroub. Preparation of superhydrophobic and oleophobic diamond nanograss array. *Journal of Materials Chemistry*, 20(47):10671–10675, 2010.

[26] Nianjun Yang, Hiroshi Uetsuka, Eiji Osawa, and Christoph E Nebel. Vertically aligned nanowires from boron-doped diamond. *Nano letters*, 8(11):3572–3576, 2008.

[27] Xinpeng Wang, Leonidas E Ocola, Ralu S Divan, and Anirudha V Sumant. Nanopatterning of ultrananocrystalline diamond nanowires. *Nanotechnology*, 23(7):075301, 2012.

[28] Sabine Szunerits, Yannick Coffinier, Elisabeth Galopin, Josef Brenner, and Rabah Boukherroub. Preparation of boron-doped diamond nanowires and their application for sensitive electrochemical detection of tryptophan. *Electrochemistry Communications*, 12(3):438–441, 2010.

[29] Chih-Hsun Hsu and Jimmy Xu. Diamond nanowire–a challenge from extremes. *Nanoscale*, 4(17):5293–5299, 2012.

[30] Daibing Luo, Liangzhuan Wu, and Jinfang Zhi. Fabrication of boron-doped diamond nanorod forest electrodes and their application in nonenzymatic amperometric glucose biosensing. *Acs Nano*, 3(8):2121–2128, 2009.

[31] Tad Whiteside, Clifford Padgett, and Amanda Mcguire. Properties of diamond nanomaterials. In *Handbook of Nanomaterials Properties*, pages 555–574. Springer, 2014.

[32] Nianjun Yang, Hiroshi Uetsuka, Eiji Osawa, and Christoph E Nebel. Vertically aligned diamond nanowires for dna sensing. *Angewandte Chemie International Edition*, 47(28):5183–5185, 2008.

[33] Nianjun Yang, Waldemar Smirnov, and Christoph E Nebel. Three-dimensional electrochemical reactions on tip-coated diamond nanowires with nickel nanoparticles. *Electrochemistry Communications*, 27:89–91, 2013.

[34] Fang Gao, Ralf Thomann, and Christoph E Nebel. Aligned pt-diamond core-shell nanowires for electrochemical catalysis. *Electrochemistry Communications*, 50:32–35, 2015.

[35] Johanna Svanberg-Larsson, Geoffrey W Nelson, Simon Escobar Steinvall, Bey F Leo, Emily Brooke, David J Payne, and John S Foord. A comparison of explicitly-terminated diamond electrodes decorated with gold nanoparticles. *Electroanalysis*, 28(1):88–95, 2016.

[36] N Aristov and A Habekost. Cyclic voltammetry-a versatile electrochemical method investigating electron transfer processes. *World Journal of Chemical Education*, 3(5):115–119, 2015.

[37] Cynthia G Zoski. *Handbook of electrochemistry*. Elsevier, 2006.

[38] Richard S Nicholson. Theory and application of cyclic voltammetry for measurement of electrode reaction kinetics. *Analytical chemistry*, 37(11):1351–1355, 1965.

[39] Donald A Dornbusch, Ramsey Hilton, Michael J Gordon, and Galen J Suppes. Effects of sonication on eis results for zinc alkaline batteries. *ECS Electrochemistry Letters*, 2(9):A89–A92, 2013.

[40] Michael C Granger and Greg M Swain. The influence of surface interactions on the reversibility of ferri/ferrocyanide at boron-doped diamond thin-film electrodes. *Journal of the Electrochemical Society*, 146(12):4551–4558, 1999.

[41] Masashi Nakamura, Narumasa Sato, Nagahiro Hoshi, and Osami Sakata. Outer helmholtz plane of the electrical double layer formed at the solid electrode–liquid interface. *ChemPhysChem*, 12(8):1430–1434, 2011.

[42] Sachiko Tanimoto and Akio Ichimura. Discrimination of inner-and outer-sphere electrode reactions by cyclic voltammetry experiments. *Journal of Chemical Education*, 90(6):778–781, 2013.

[43] Wolfgang Rathmann and Guido Giani. Global prevalence of diabetes: estimates for the year 2000 and projections for 2030. *Diabetes care*, 27(10):2568–2569, 2004.

[44] Jianwen Zhao, Liangzhuan Wu, and Jinfang Zhi. Non-enzymatic glucose detection using as-prepared boron-doped diamond thin-film electrodes. *Analyst*, 134(4):794–799, 2009.

[45] Joowook Lee and Su-Moon Park. Direct electrochemical assay of glucose using boron-doped diamond electrodes. *Analytica chimica acta*, 545(1):27–32, 2005.

[46] Takeshi Watanabe, Tribidasari A Ivandini, Yoshihiro Makide, Akira Fujishima, and Yasuaki Einaga. Selective detection method derived from a controlled diffusion process at metal-modified diamond electrodes. *Analytical chemistry*, 78(22):7857–7860, 2006.

[47] Kathryn E Toghill, Lei Xiao, Michael A Phillips, and Richard G Compton. The non-enzymatic determination of glucose using an electrolytically fabricated nickel microparticle modified boron-doped diamond electrode or nickel foil electrode. *Sensors and actuators B: Chemical*, 147(2):642–652, 2010.

[48] Takeshi Watanabe and Yasuaki Einaga. Design and fabrication of nickel microdisk-arrayed diamond electrodes for a non-enzymatic glucose sensor based on control of diffusion profiles. *Biosensors and Bioelectronics*, 24(8):2684–2689, 2009.

[49] Tribidasari A Ivandini, Rika Sato, Yoshihiro Makide, Akira Fujishima, and Yasuaki Einaga. Electroanalytical application of modified diamond electrodes. *Diamond and related materials*, 13(11):2003–2008, 2004.

[50] Qi Wang, Palaniappan Subramanian, Musen Li, Weng Siang Yeap, Ken Haenen, Yannick Coffinier, Rabah Boukherroub, and Sabine Szunerits. Non-enzymatic glucose sensing on long and short diamond nanowire electrodes. *Electrochemistry Communications*, 34:286–290, 2013.

[51] Siriwan Nantaphol, Takeshi Watanabe, Naohiro Nomura, Weena Siangproh, Orawon Chailapakul, and Yasuaki Einaga. Bimetallic pt–au nanocatalysts electrochemically deposited on boron-doped diamond electrodes for nonenzymatic glucose detection. *Biosensors and Bioelectronics*, 2017.

[52] Andrea C Ferrari. Raman spectroscopy of graphene and graphite: disorder, electron–phonon coupling, doping and nonadiabatic effects. *Solid state communications*, 143(1):47–57, 2007.

[53] Satoshi Koizumi, Christoph Nebel, and Milos Nesladek. *Physics and applications of CVD diamond*. John Wiley & Sons, 2008.

[54] Michael C Granger, Malgorzata Witek, Jishou Xu, Jian Wang, Mateusz Hupert, Amy Hanks, Miles D Koppang, James E Butler, Guy Lucazeau, Michel Mermoux, et al. Standard electrochemical behavior of high-quality, boron-doped polycrystalline diamond thin-film electrodes. *Analytical Chemistry*, 72(16):3793–3804, 2000.

[55] William R LaCourse and Dennis C Johnson. Optimization of waveforms for pulsed amperometric detection of carbohydrates based on pulsed voltammetry. *Analytical Chemistry*, 65(1):50–55, 1993.

[56] Serhiy Cherevko and Chan-Hwa Chung. Gold nanowire array electrode for non-enzymatic voltammetric and amperometric glucose detection. *Sensors and Actuators B: Chemical*, 142(1):216–223, 2009.

[57] Aiping Liu, Qinghua Ren, Tao Xu, Ming Yuan, and Weihua Tang. Morphology-controllable gold nanostructures on phosphorus doped diamond-like carbon surfaces and their electrocatalysis for glucose oxidation. *Sensors and Actuators B: Chemical*, 162(1):135–142, 2012.

[58] W Smirnov, A Kriele, N Yang, and CE Nebel. Aligned diamond nano-wires: Fabrication and characterisation for advanced applications in bio-and electrochemistry. *Diamond and Related Materials*, 19(2):186–189, 2010.

[59] Fathi Habashi. *Kinetics and mechanism of gold and silver dissolution in cyanide solution*. Montana College of Mineral Science and Technology, 1967.

[60] Henry Oliver Lancaster and Eugene Seneta. *Chi-square distribution*. Wiley Online Library, 1969.

[61] Kathryn E Toghill and Richard G Compton. Electrochemical non-enzymatic glucose sensors: a perspective and an evaluation. *Int. J. Electrochem. Sci*, 5(9):1246–1301, 2010.

[62] Rafiq Ahmad, Nirmalya Tripathy, Min-Sang Ahn, Kiesar Sideeq Bhat, Tahmineh Mahmoudi, Yousheng Wang, Jin-Young Yoo, Dae-Wook Kwon, Hwa-Young Yang, and Yoon-Bong Hahn. Highly efficient non-enzymatic glucose sensor based on cuo modified vertically-grown zno nanorods on electrode. *Scientific Reports*, 7, 2017.

A

Ferrocyanide

Measurements with different scan rates are proceeded to see if there is a linear relationship between the square root of the scan rate and the peak current values. All graphs of this linear fitting are shown in Figure A.2.

There are also measurements done with different molarities of ferrocyanide to see what the relation between the peak currents and the molarities is, as is shown in Figure A.3.

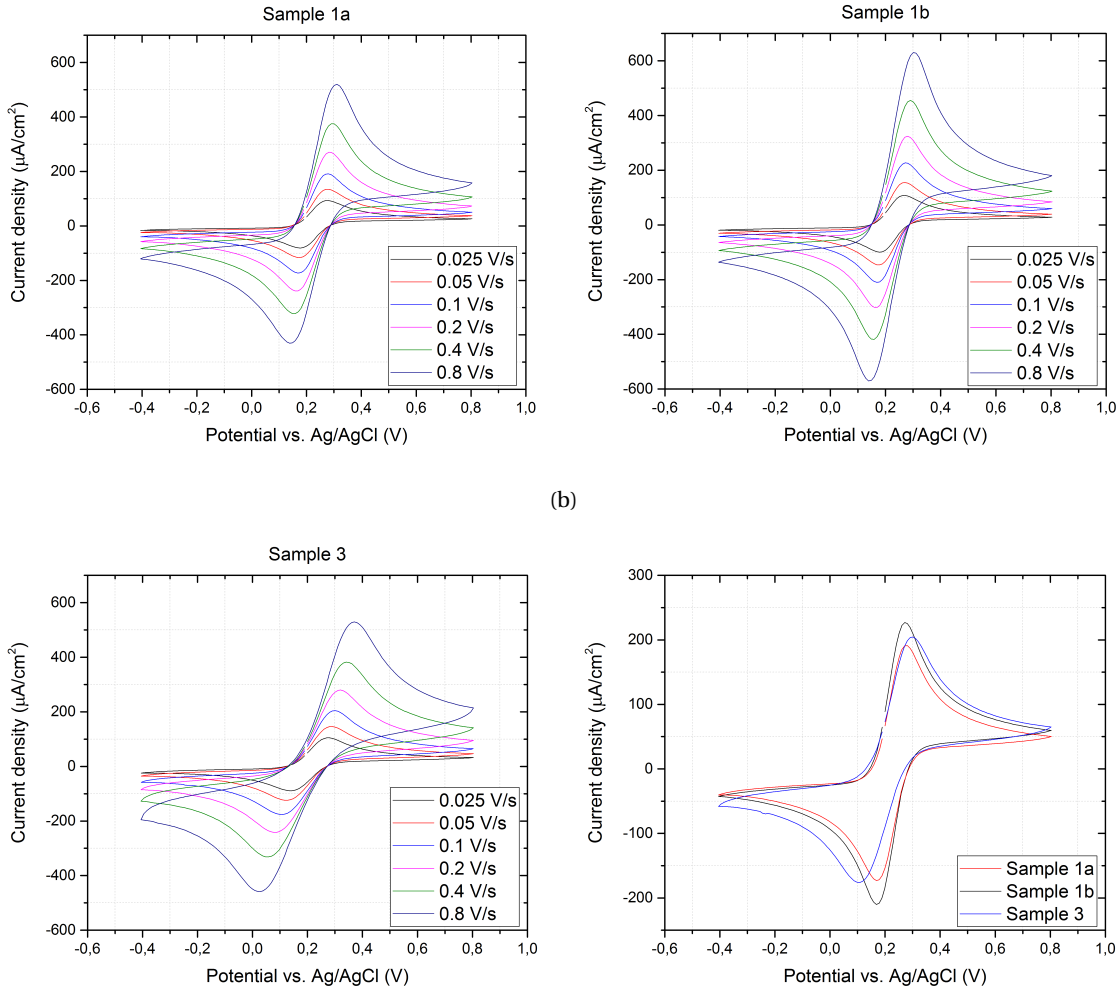

Figure A.1: a), b) and c) show CVs of diamond electrodes 1a, 1b and 3 in 1 mM ferrocyanide and 0.1 M KCl at different scan rates, 10th cycle is shown. d) shows the CVs of these three samples in one figure with a scan rate of 0.1 V/s

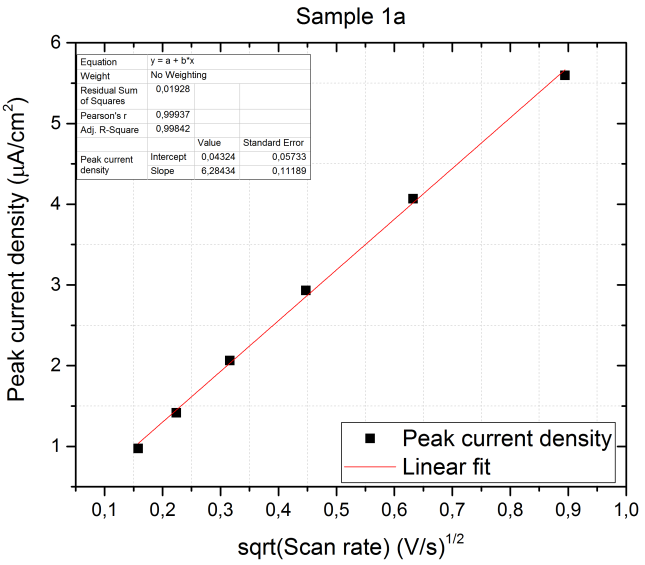

(a)

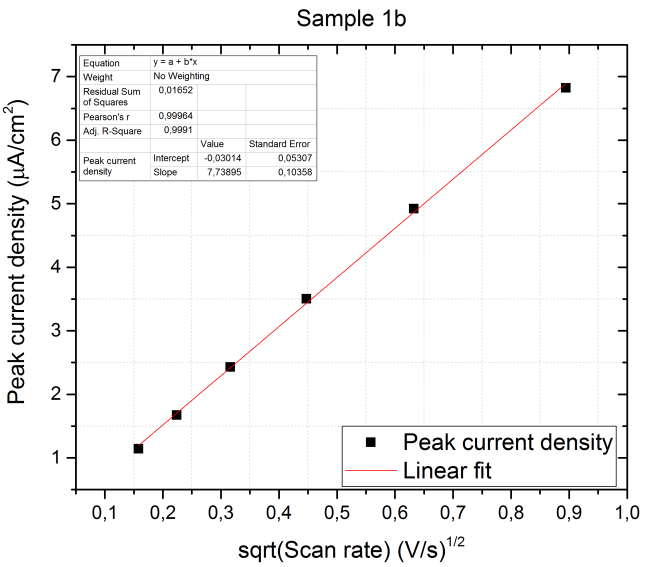

(b)

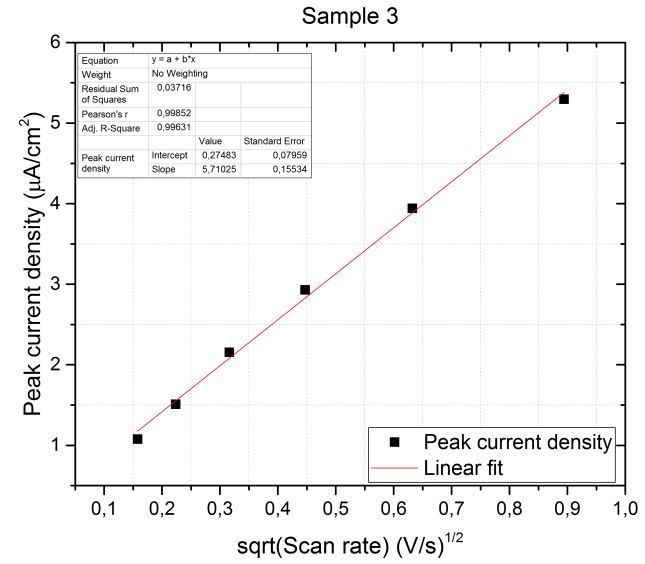

(c)

Figure A.2: Linear fitting of peak current densities with the square root of the scan rate

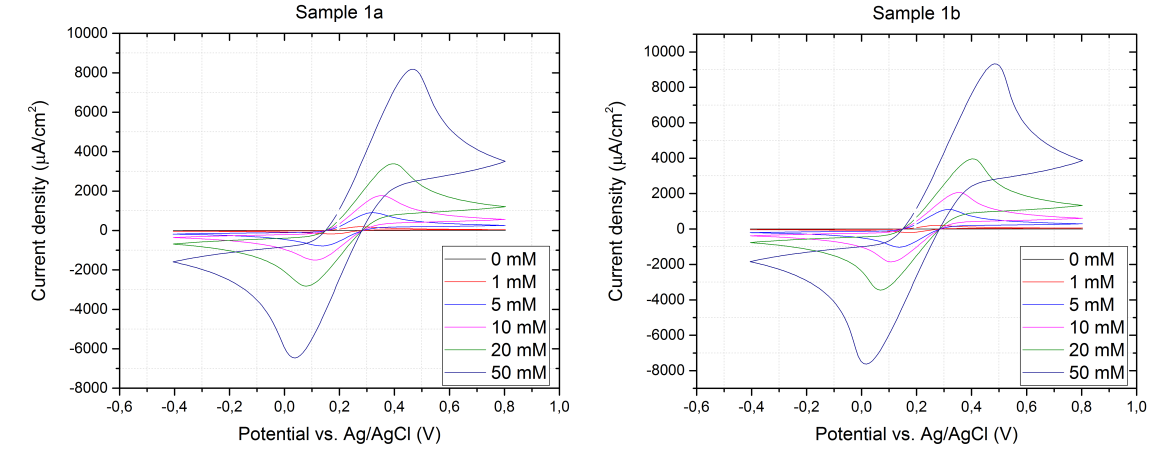

(a)

(b)

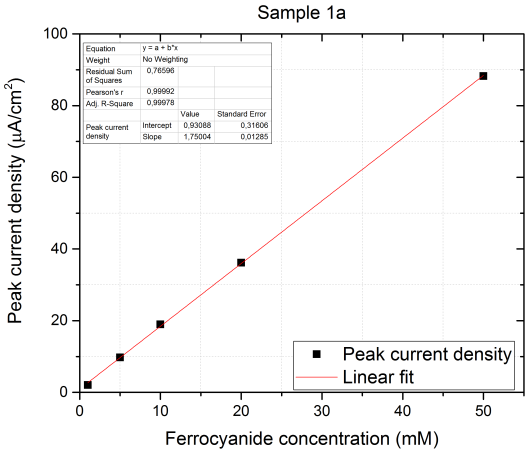

(c)

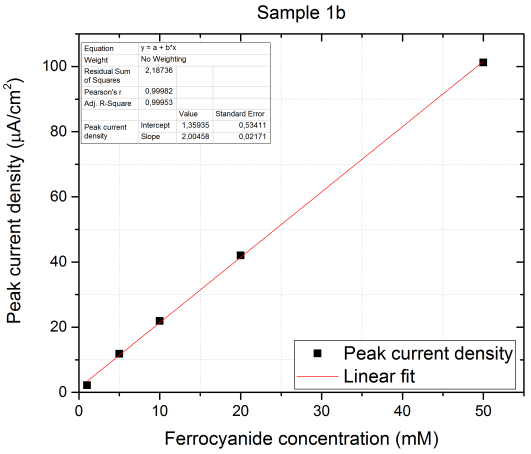

(d)

Figure A.3: a) and b) show CVs of electrodes 1a and 1b in different molarities of ferrocyanide and 0.1 *M* KCl. c) and d) show the linear fitting of peak current densities with the molarities

B

Ruhex

Measurements with different scan rates are proceeded to see if there is a linear relationship between the square root of the scan rate and the peak current values. All graphs of the measurements at different scan rates are shown in Figure B.1. The linear fitting of these measurements is shown in Figure B.2.

There are also measurements done with different molarities of ruhex to see what the relation between the peak currents and the molarities is, as is shown in Figure B.3.

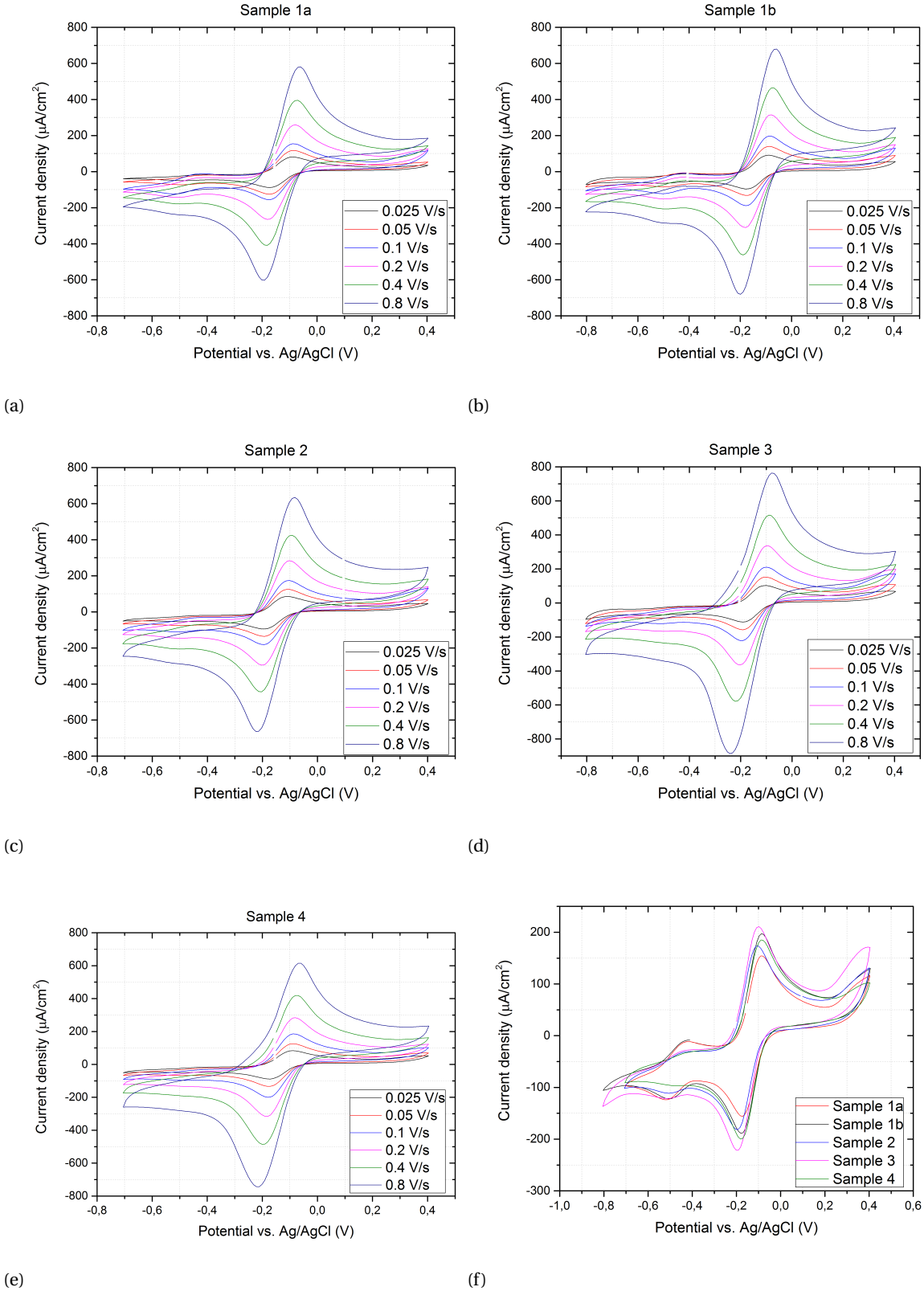

Figure B.1: Figure a-f) CVs of the different diamond electrodes in 1 mM ruhex and 0.1 M KCl at different scan rates, 10th cycle is shown. Measurements of Figure f) are performed with a scan rate of 0.1 V/s

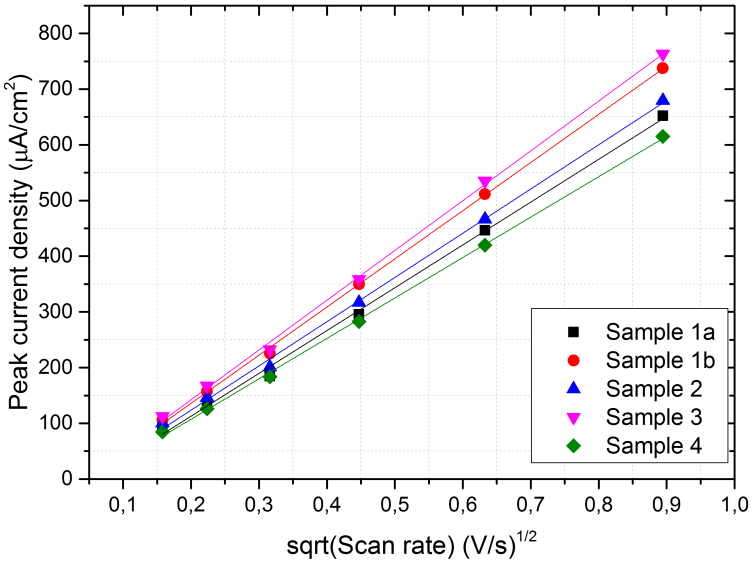

(a)

Equation	y = a + b*x				
Weight	No Weighting				
Residual Sum of Squares	576,0904	171,13182	375,40066	328,90315	162,91357
Pearson's r	0,99874	0,9997	0,99923	0,99947	0,9996
Adj. R-Square	0,99684	0,99926	0,99807	0,99867	0,999
		Value	Standard Error		
Peak current density	Intercept	-40,96862	9,90907		
	Slope	768,77892	19,34053		
	Intercept	-37,20108	5,40074		
	Slope	864,92056	10,54116		
	Intercept	-35,26567	7,99899		
	Slope	794,2584	15,61243		
	Intercept	-36,64989	7,48724		
	Slope	893,99674	14,61359		
	Intercept	-37,87618	5,26946		
	Slope	725,83256	10,28494		

(b)

Figure B.2: Linear fitting of peak current densities with the square root of the scan rates

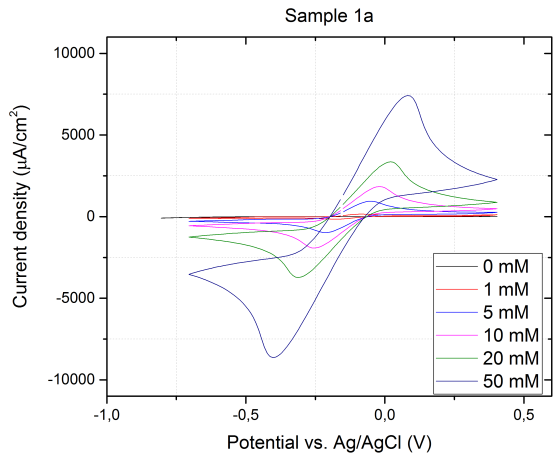

(a)

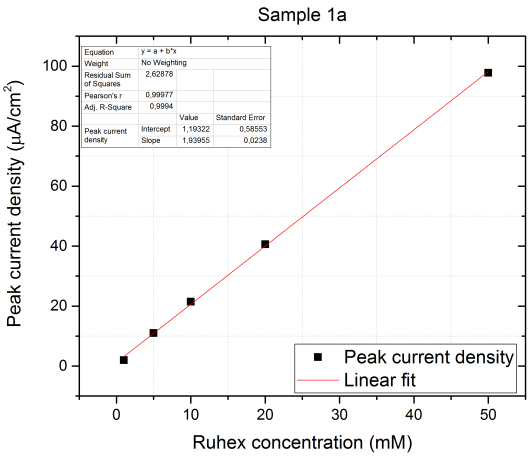

(b)

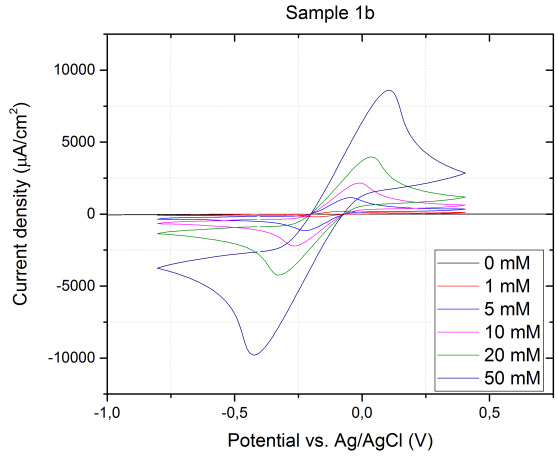

(c)

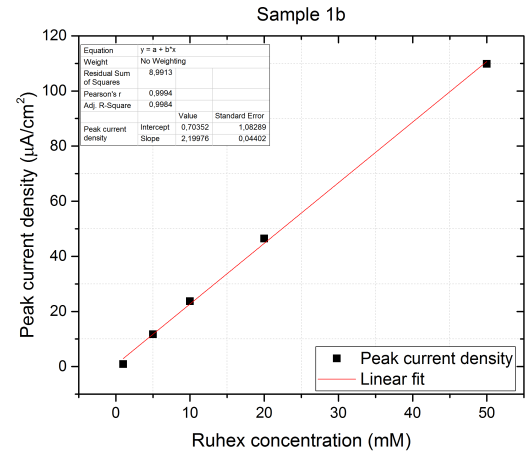

(d)

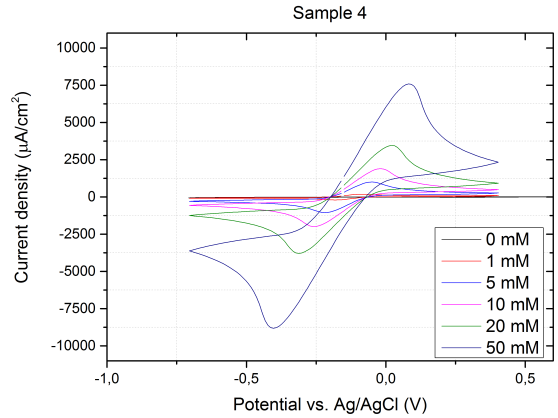

(e)

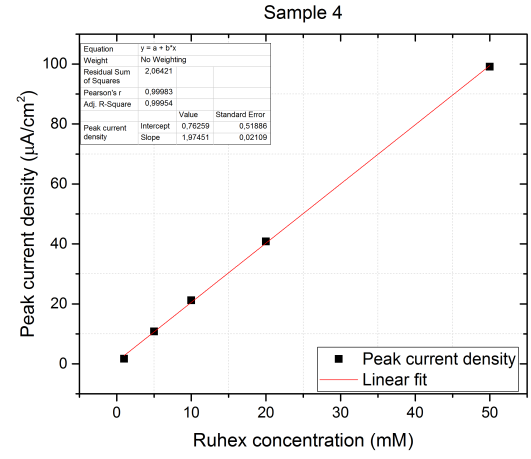

(f)

Figure B.3: a), c) and e) show CVs of the different electrodes in different molarities of ruhex of 0.1 M KCl at a scan rate of 0.1 V/s, 10th cycle is shown. b), d) and f) show the linear fittings of peak current densities with the molarities

C

Kinetics and EIS-data

All electrochemical impedance spectroscopy fitting results are shown in Table C.1. All data are fitted to the Randles circuit, which is already described in Subsection 2.3. All measurements are performed with the same variables. The frequency is taken from 0.1 to 100000 Hz, the amplitude is 0.01, the integration time is 0.125 s and the number of points taken is 50. The only variable that has different values per measurement is the formal potential, this is changed in advance of each EIS measurement.

Table C.1: EIS results of different electrodes in $1\,mM$ ferrocyanide and $1\,mM$ ruhex at a temperature of $293K$ and a scan rate of 100 mV/s

Analyte	Sample	R_S in Ω	R_{CT} in Ω	Q_0 in μF	n_{CPE}	W in $\mu\Omega \cdot s^{-1/2}$	χ^2	k_0 in $\mu m/s$
$Fe(CN)_6^{3-/4-}$	1a	183.9	435.5	3.06	0.93	587.1	$2.13 \cdot 10^{-3}$	27.60
	1b	181.5	132.6	3.51	0.93	693.1	$8.95 \cdot 10^{-4}$	90.50
	3	185.6	1218	13.88	0.92	639.2	$1.053 \cdot 10^{-2}$	9.85
$Ru(NH_3)_6^{2+/3+}$	1a	195.6	80.96	209.4	0.63	463.3	$5.70 \cdot 10^{-4}$	148
	1b	187.1	77.32	245.7	0.63	524.8	$3.22 \cdot 10^{-4}$	155
	2	186.7	103	216	0.67	479	$3.34 \cdot 10^{-4}$	117
	3	183.6	18.65	37.19	0.91	710.4	$1.22 \cdot 10^{-4}$	644
	4	190.3	11.25	34.5	0.90	639.1	$2.66 \cdot 10^{-4}$	1070

D

Glucose

Measurements with different scan rates are proceeded, Figure D.1, to see if there is a linear relationship between the square root of the scan rate and the peak current values. All graphs of this linear fitting are shown in Figure D.3a. When all data of sample 1b are used for the linear fitting between the peak currents and the square root of the scan rate the fitting is really poor, as is shown in Figure D.2. After removing the data points for the two slowest scan rates, 0.025 V/s and 0.05 V/s, the linear fit is good.

There are also measurements done with different molarities of glucose to see what the relation between the peak currents and the molarities is, as is shown in Figure D.3b.

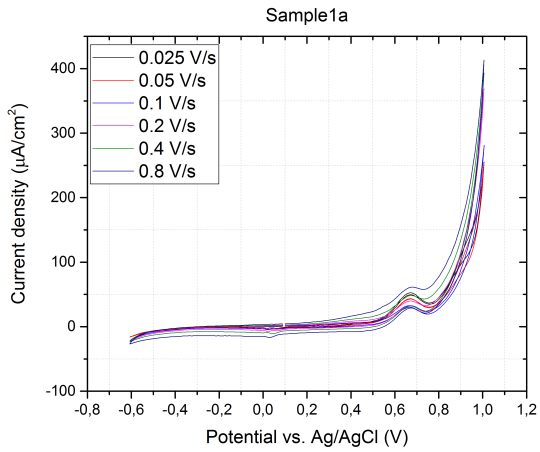

(a)

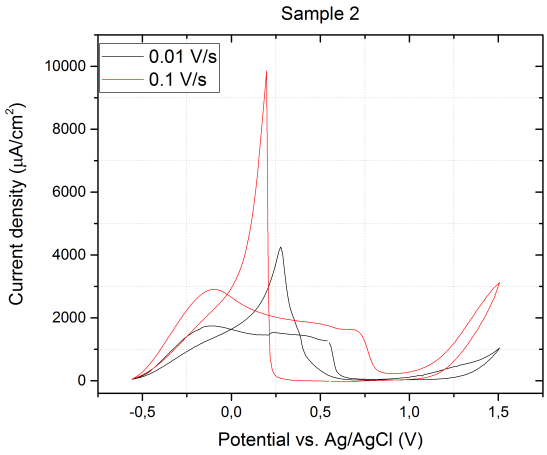

(b)

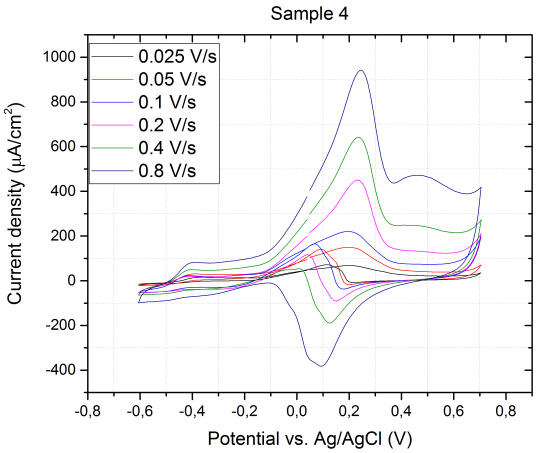

(c)

Figure D.1: CVs in 0.1 M NaOH and glucose at different scan rates, 10th cycle is shown. a) CV of sample 1a with 1 mM glucose, b) CV of sample 2 with 200 mM glucose, c) CV of sample 4 with 1 mM glucose

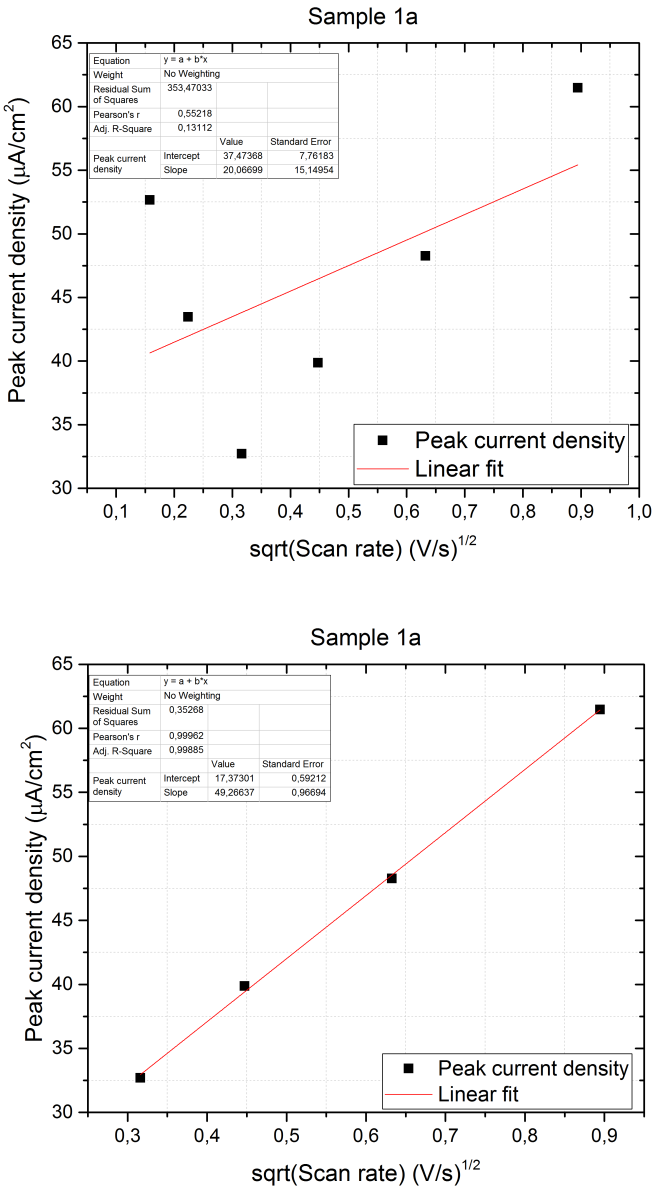

Figure D.2: Linear fitting of peak current values with the square root of the scan rate for sample 1a. a) shows the linear fit of scan rates from 0.025 V/s to 0.8 V/s, b) shows the linear fit of scan rates from 0.1 V/s to 0.8 V/s

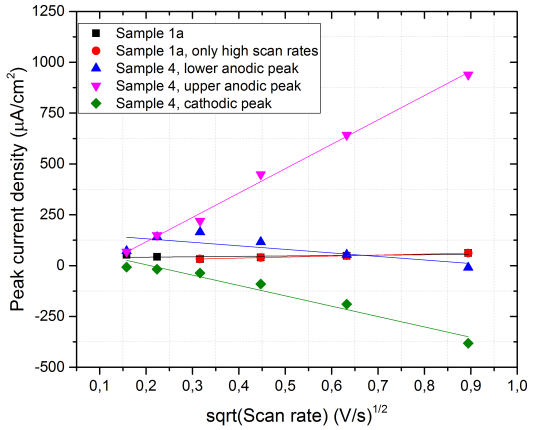

(a)

Equation	y = a + b*x				
Weight	No Weighting				
Residual Sum of Squares	353,47033	0,35268	8751,31787	2751,15243	4284,22845
Pearson's r	0,55218	0,99962	-0,75595	0,99752	-0,97926
Adj. R-Square	0,13112	0,99885	0,46432	0,99382	0,94869
		Value	Standard Error		
Peak current density	Intercept	37,47368	7,76183		
	Slope	20,06699	15,14954		
	Intercept	17,37301	0,59212		
	Slope	49,26637	0,96694		
	Intercept	166,99873	38,62108		
	Slope	-174,09341	75,38063		
	Intercept	-122,68256	21,65434		
	Slope	1198,94711	42,26495		
	Intercept	106,38444	27,0224		
	Slope	-509,86931	52,74233		

(b)

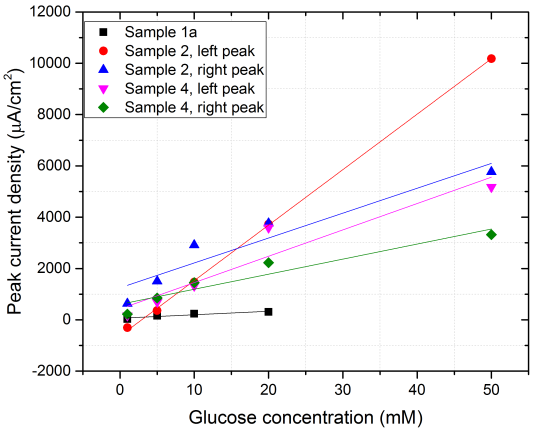

(c)

Equation	y = a + b*x				
Weight	No Weighting				
Residual Sum of Squares	4436,23152	2,56209E6	1,06341E6	1,59732E6	513431,35428
Pearson's r	0,94534	0,98446	0,98555	0,95442	0,95507
Adj. R-Square	0,84051	0,95887	0,96174	0,88122	0,88288
		Value	Standard Error		
Peak current density	Intercept	55,5102	37,99962		
	Slope	13,58623	3,31372		
	Intercept	1837,58908	578,05479		
	Slope	228,13251	23,49739		
	Intercept	1071,17722	372,41072		
	Slope	152,55369	15,13815		
	Intercept	522,05295	456,42355		
	Slope	102,75961	18,55319		
	Intercept	567,3113	258,76941		
	Slope	58,70885	10,51873		

(d)

Figure D.3: Linear fitting of peak currents with the a) and b) square root of the scan rates, c) and d) and the molarities